J. Fluid Mech. (2003), *vol.* 491, *pp.* 65–100.
DOI: 10.1017/S0022112003005299 Printed in the United Kingdom

Roles of non-aligned eigenvectors of strain-rate and subgrid-scale stress tensors in turbulence generation

By KIYOSI HORIUTI

Department of Mechano-Aerospace Engineering, Tokyo Institute of Technology, 2-12-1 O-okayama, Meguro-ku, Tokyo 152-8552, Japan

(Received 3 September 2002 and in revised form 24 March 2003)

Alignment of the eigenvectors for strain-rate tensors and subgrid-scale (SGS) stress tensors in large-eddy simulation (LES) is studied in homogeneous isotropic turbulence. Non-alignment of these two eigenvectors was shown in Tao, Katz & Meneveau (2002). In the present study, the specific term in the decomposition of the SGS stress tensor, which is primarily responsible for causing this non-alignment, is identified using the nonlinear model. The bimodal behaviour of the alignment configuration reported in Tao *et al.* (2002) was eliminated by reordering the eigenvalues according to the degree of alignment of the corresponding eigenvectors with the vorticity vector. The preferred relative orientation of the eigenvectors was $\approx 42^\circ$. The alignment trends were conditionally sampled based on the relative dominance of strain and vorticity. The effect of the identified term on the alignment was the largest in the region in which the magnitudes of strain and vorticity were comparable and large (flat sheet). The most probable alignment configuration in the flat-sheet region was different from those in the strain-dominated and vorticity-dominated regions. The relative orientation of the eigenvectors was dependent on the degree of resolution for the flat sheet region yielded on the LES mesh. When the alignment was conditionally sampled on the events with the backward scatter of the SGS energy into the grid scale, the interchange of the alignment of the eigenvectors took place. Relevance of the identified term for the generation of turbulence is investigated. It is shown that the identified term makes no contribution to the production of the total SGS energy, but contributes significantly to the generation of the SGS enstrophy. The identified term causes a time-lag in the evolution of the turbulent energy and enstrophy. It is shown that generation of vorticity is markedly attenuated when the magnitude of the identified term is modified, and the original nonlinear model yielded the results which are in the closest agreement with the direct numerical simulation data.

1. Introduction

Since turbulence consists of eddies with a very wide size range, when we consider simulating the turbulence numerically, a vast number of degrees of freedom is required to resolve up to the small eddies in which molecular dissipation of the turbulent energy takes place. To reduce the number of degrees of freedom, the small scales should be coarsely grained. One of the methods available for this reduction is large-eddy simulation (LES). In LES, a coarse graining of the small scales is performed by

applying a filtering operation to the raw variable f

$$\overline{f}(\boldsymbol{x}) = \int_D \overline{G}(\boldsymbol{x} - \boldsymbol{x}'') f(\boldsymbol{x}'')\, \mathrm{d}\boldsymbol{x}'', \tag{1.1}$$

where $\overline{f}$ denotes the resolved or grid scale component, $\overline{G}(\boldsymbol{x})$ the filter function, D the flow domain, and $\boldsymbol{x} = (x_1, x_2, x_3)$. The velocity and pressure fields (f) are decomposed into the grid scale component ($\overline{f}$), and the subgrid-scale (SGS) component (f') through this filtering procedure. The filtered Navier–Stokes equations are derived by applying the filtering operation (1.1) to the Navier–Stokes equations as

$$\frac{\partial \overline{u}_i}{\partial t} + \frac{\partial (\overline{u}_i \overline{u}_j)}{\partial x_j} = -\frac{\partial \tau_{ij}}{\partial x_j} - \frac{\partial \overline{p}}{\partial x_i} + \nu \frac{\partial^2 \overline{u}_i}{\partial x_k \partial x_k}, \tag{1.2}$$

where $\overline{u}_i$ $(i = 1, 2, 3)$ denotes the grid-scale velocity field, $\overline{p}$ denotes the grid-scale pressure, and ν denotes the kinematic viscosity. The subgrid-scale (SGS) stress tensor, $\tau_{ij} = (\overline{u_i u_j} - \overline{u}_i \overline{u}_j)$, results from coarse graining of the SGS. For recent reviews of LES, see, e.g. Piomelli (1999) and Meneveau & Katz (2000).

Approximation of the SGS stress tensor has been commonly carried out using the eddy viscosity coefficient model, in which a complete alignment of the SGS stress tensor with the grid-scale strain-rate tensor is assumed. A representative model is the Smagorinsky model (Smagorinsky 1963):

$$\tau_{ij} \simeq \tfrac{2}{3}\overline{E}_G \delta_{ij} - 2\nu_e \overline{S}_{ij}, \tag{1.3}$$

where ν_e is the isotropic eddy viscosity coefficient,

$$\nu_e = C_S \overline{\Delta}^2 |\overline{S}|, \; |\overline{S}| = [2\overline{S}_{ij}\overline{S}_{ij}]^{1/2}, \quad \overline{S}_{ij} = \frac{1}{2}\left(\frac{\partial \overline{u}_i}{\partial x_j} + \frac{\partial \overline{u}_j}{\partial x_i}\right).$$

C_S is a model constant, $\overline{E}_G$ is the SGS energy $(\overline{u_i u_i} - \overline{u}_i \overline{u}_i)/2$, and $\overline{\Delta}$ is the characteristic SGS length scale. Here, as well as in the following, the SGS stress tensor, τ_{ij}, was forced to be trace-free, and the deviatoric part $(\tau_{ij} - \delta_{ij}\tau_{kk}/3)$ is denoted as τ_{ij} for brevity.

Assessment of the eddy-viscosity model using the direct numerical simulation (DNS) data, however, showed that its accuracy for approximation of the τ_{ij} term is generally low, i.e. the correlation coefficient, ρ, between the exact τ_{ij} term and the τ_{ij} term modelled using the Smagorinsky model was typically $\rho \approx 0.2$ (e.g. Clark, Ferziger & Reynolds 1979). In fact, non-alignment of the eigenvectors for the strain-rate and SGS stress tensors was shown in Tao, Katz & Meneveau (2000), in which the three-dimensional velocity distributions measured using holographic particle image velocimetry were used to assess the alignment. The most extensive SGS stress eigenvector was shown to be preferentially aligned at $\approx 34^\circ$ to the most contracting strain-rate eigenvector. In Tao, Katz & Meneveau (2002), the experimental data for more statistical samples were used, and the angle was $\approx 32^\circ$. The observed trend for alignment was confirmed in the DNS data for homogeneous isotropic turbulence. It was also shown that the alignment angle is increased to $\approx 55^\circ$ when an intense backward scatter of the SGS energy into the grid scale takes place. In addition, the alignment of the SGS stress eigenvector and the strain-rate eigenvector showed a bimodal behaviour, one in which the most extensive stress eigenvector is preferentially aligned with the extensive strain-rate eigenvector (denoted the $\alpha\beta\gamma - \alpha\beta\gamma$ configuration in Tao *et al.* 2002), and the other in which the most extensive stress eigenvector is preferentially aligned with the intermediate strain-rate eigenvector

(the $\alpha\beta\gamma - \beta\alpha\gamma$ configuration). It was revealed that the primary element of the SGS stress tensor which causes this non-alignment is the modified Leonard term in the decomposition of the τ_{ij} term.

An alternative SGS model is the scale-similarity model, in which the SGS primitive variables (e.g. velocity components) are directly modelled using the synthetic velocities, e.g. as (Bardina 1983)

$$\tau_{ij} \simeq (\overline{\overline{u}_i \overline{u}_j} - \overline{\overline{u}}_i \, \overline{\overline{u}}_j), \tag{1.4}$$

where the grid-scale velocities, $\overline{u}_i$, were used as the synthetic velocities. Different definitions for the synthetic velocities have been considered (e.g. Domaradzki & Saiki 1997). This model yields a much higher correlation with the exact SGS stress tensor than the SGS eddy viscosity model (e.g. Clark *et al.* 1979; Piomelli 1999). When the SGS production term, P,

$$P = -\tau_{ij} \overline{S}_{ij}, \tag{1.5}$$

was considered, however, the eddy viscosity model showed a much better performance than that at the tensorial level of the SGS stress, τ_{ij}, i.e. ρ was increased to typically ≈ 0.6 (e.g. Clark *et al.* 1979; Liu, Meneveau & Katz 1994; Piomelli 1999). In practice, the SGS eddy viscosity model has been added to the scale-similarity model to yield sufficient drain of the grid-scale energy into the SGS.

The lowest-order approximation of the scale-similarity model, equation (1.4), using the Taylor expansion as the nonlinear model is

$$\tau_{ij} \simeq \frac{\overline{\Delta}^2}{12} \frac{\partial \overline{u}_i}{\partial x_k} \frac{\partial \overline{u}_j}{\partial x_k}, \tag{1.6}$$

which exhibits a good performance for predicting the SGS stress (Clark *et al.* 1979; Liu *et al.* 1994). In Tao *et al.* (2002), it was shown that the stress eigenvectors of the nonlinear model are preferentially aligned in the same direction as those of the measured stress eigenvectors. Stresses computed using the nonlinear model had a bimodal behaviour, but the preferred angles were 42° instead of the measured 32°.

The aim of the present study is to identify the specific term which is responsible for causing the non-alignment, clarify the roles of this identified term for the generation of turbulence, and demonstrate the limitations of the SGS eddy viscosity model. In § 2, the configuration of alignment between the eigenvectors for the strain-rate and the SGS stress tensors is discussed, and the results are compared with those obtained in Tao *et al.* (2002). In § 3, the element in the decomposition of the SGS stress tensor which is primarily responsible for causing the non-alignment of the two eigenvectors is identified, and its influence on the SGS production term is examined. The limitation of the SGS eddy viscosity model is discussed. Section 4 thoroughly analyses the characteristics of the identified term. The impact of the identified term for generation of the SGS turbulent energy and enstrophy is shown. Throughout §§ 2, 3 and 4, the analysis was carried out in an *a priori* manner (Piomelli 1999) using the direct numerical simulation data for the homogeneous isotropic turbulence. Section 5 describes the elucidation of the role of the identified term in an *a posteriori* manner by incorporating the SGS models into the actual LES of ABC flow. Dependence of temporal evolution of turbulence statistics and structures on the modification of the identified term is examined, and the relevance of the identified term is revealed. Our conclusions are given in § 6. In the Appendix, the nonlinear models which were considered in the present study are compared with those used in the previous studies.

2. Determination of alignment configuration

In the present study, the Gaussian function

$$\overline{G}(\boldsymbol{x}) = \overline{G}(x_1, x_2, x_3) = \left(\sqrt{\frac{6}{\pi}}\,\frac{1}{\overline{\Delta}}\right)^3 \exp\left(\frac{-6\left(x_1^2 + x_2^2 + x_3^2\right)}{\overline{\Delta}^2}\right), \tag{2.1}$$

was used as the filter function, $\overline{G}(\boldsymbol{x})$, in (1.1), where the characteristic filter width, $\overline{\Delta}$, is chosen to be equal to 2Δ in the present study. Δ is the grid interval for the LES mesh.

We have used the direct numerical simulation (DNS) data for incompressible decaying homogeneous isotropic turbulence, which was generated with 256, 256 and 256 grid points, respectively, in the x-, y- and z-directions. Periodic boundary conditions were imposed in the three directions. The size of the computational domain was 2π in each direction, the viscosity $\nu = 0.00014$, and the time interval, Δt, was set equal to 0.0005. For details of the DNS data, see Horiuti (2001). Assessment was performed using the data at the instant when the Reynolds number based on the Taylor microscale, $R_\lambda \approx 87.6$. The LES data were generated by applying the Gaussian filter to the DNS data, and were truncated to $64 \times 64 \times 64$ grid points in the x-, y- and z-directions, respectively, unless otherwise stated. The Kolmogorov length, η, of the DNS data was ≈ 0.0081, and $k_{max}\eta \approx 1.03$ (k_{max} is the maximum wavenumber). When the DNS data were truncated to 64^3 grid points, $\Delta/\eta = 12.2(\overline{\Delta}/\eta = 24.4)$.

The eigenvalues for the (grid-scale) strain-rate tensor, $\overline{S}_{ij}$, are denoted as σ_i ($i = 1, 2, 3$). In Tao *et al.* (2000, 2002), the descending ordering of these eigenvalues, such that $\sigma_1 \geqslant \sigma_2 \geqslant \sigma_3$, was used. The eigenvectors corresponding to the eigenvalues, σ_i, are denoted as $\boldsymbol{e}_i$ ($i = 1, 2, 3$). The same ordering of the eigenvalues and of the corresponding eigenvectors was used for other eigenvalues. The eigenvalues for the SGS stress tensor, $(-\tau_{ij})$, are denoted by $(-\tau)_i$ ($i = 1, 2, 3$) and the eigenvectors corresponding to those eigenvalues are denoted by $(-\boldsymbol{\tau})_i$ ($i = 1, 2, 3$).

Figure 1 shows the joint probability density function (p.d.f.) of the alignment between the stress eigenvector $(-\boldsymbol{\tau})_1$ and the strain-rate eigenvector $\boldsymbol{e}_1$, $\cos\theta[(-\boldsymbol{\tau})_1 - \boldsymbol{e}_1]$, and alignment between $(-\boldsymbol{\tau})_2$ and $\boldsymbol{e}_2$, $\zeta[(-\boldsymbol{\tau})_2 - \boldsymbol{e}_2^P]$. In the present study, the same notation for the angles, θ, ζ, ϕ, as that used in Tao *et al.* (2002) is used, that is, $\theta[(-\boldsymbol{\tau})_3 - \boldsymbol{e}_3]$ denotes the angle between the eigenvectors $(-\boldsymbol{\tau})_3$ and $\boldsymbol{e}_3$, $\zeta[(-\boldsymbol{\tau})_2 - \boldsymbol{e}_2^P]$ denotes the angle between $(-\boldsymbol{\tau})_2$ and the eigenvector $\boldsymbol{e}_2^P$ on the $((-\boldsymbol{\tau})_1, (-\boldsymbol{\tau})_2)$-plane, and $\boldsymbol{e}_2^P$ is the projection of $\boldsymbol{e}_2$ on this plane. $\phi[(-\boldsymbol{\tau})_3^P - \boldsymbol{e}_1]$ denotes the angle between $\boldsymbol{e}_1$ and the eigenvector $(-\boldsymbol{\tau})_3^P$ on the $(\boldsymbol{e}_1, \boldsymbol{e}_2)$-plane, and $(-\boldsymbol{\tau})_3^P$ is the projection of $(-\boldsymbol{\tau})_3$ on this plane. Figure 2 shows the sketch for definitions of these angles, θ, ζ and ϕ. The joint p.d.f.s were computed by using 20×20 bins of equal width in both directions. The bimodal behaviour of alignment between the strain-rate and stress tensor eigenvectors which was pointed out in Tao *et al.* (2002) can be seen in figure 1. The two peaks can be identified in figure 1. The first one is located at $\cos\theta[(-\boldsymbol{\tau})_1 - \boldsymbol{e}_1] \approx 0$ (i.e. $\theta[(-\boldsymbol{\tau})_1 - \boldsymbol{e}_1] \approx \pi/2$), and $\zeta[(-\boldsymbol{\tau})_2 - \boldsymbol{e}_2^P] \approx \pi/2$. The second one is located at $\cos\theta[(-\boldsymbol{\tau})_1 - \boldsymbol{e}_1] \approx 0.75$ (i.e. $\theta[(-\boldsymbol{\tau})_1 - \boldsymbol{e}_1] \approx 42^\circ$), and $\zeta[(-\boldsymbol{\tau})_2 - \boldsymbol{e}_2^P] \approx 0$. The first peak corresponds to the $\alpha\beta\gamma - \beta\alpha\gamma$ configuration defined in Tao *et al.* (2002), and the second peak to the $\alpha\beta\gamma - \alpha\beta\gamma$ configuration. Another peak is discernible at $\cos\theta[(-\boldsymbol{\tau})_1 - \boldsymbol{e}_1] \approx 1$ (i.e. $\theta[(-\boldsymbol{\tau})_1 - \boldsymbol{e}_1] \approx 0$), and $\zeta[(-\boldsymbol{\tau})_2 - \boldsymbol{e}_2^P] \approx 0$. The alignment configuration corresponding to this peak will be discussed in § 3.

In the present paper, only the results for two-dimensional joint p.d.f.s are shown. Those for three-dimensional joint p.d.f.s were similar to those presented in Tao *et al.* (2002) except for the amplitude of the alignment angle. The most probable

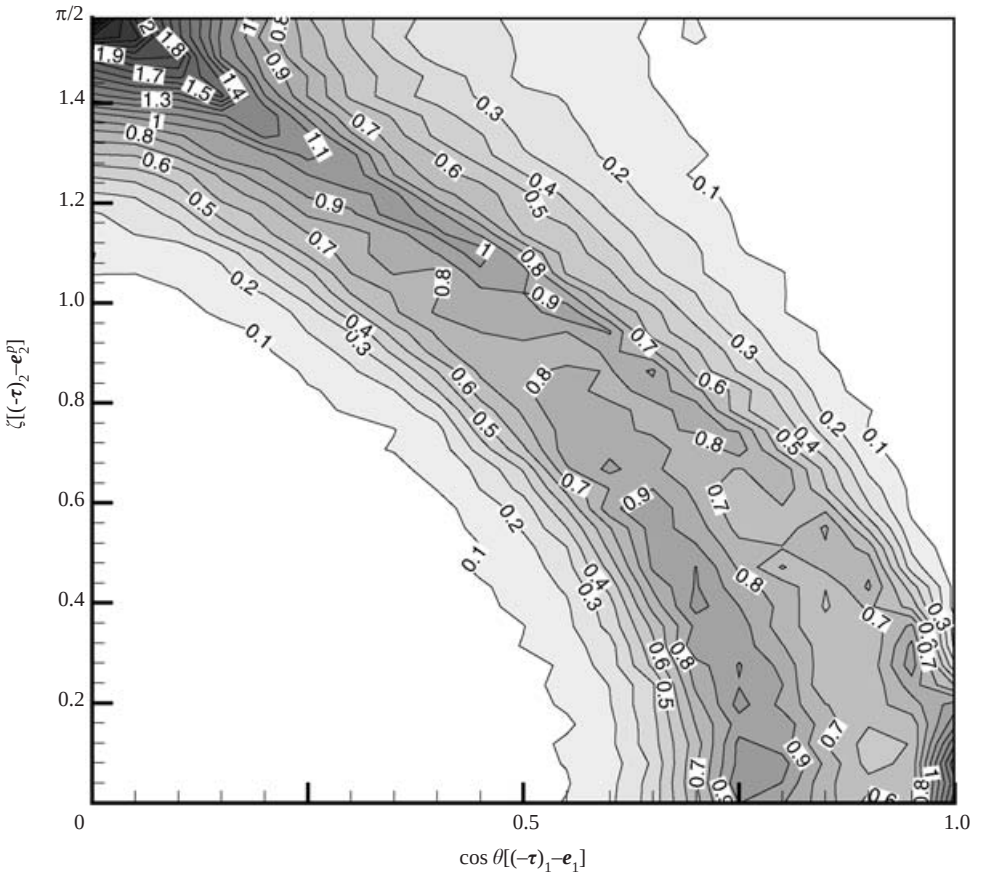

FIGURE 1. Joint p.d.f. of the alignment between the eigenvector $(-\boldsymbol{\tau})_1$ and the strain-rate eigenvector $\boldsymbol{e}_1$, $\cos\theta[(-\boldsymbol{\tau})_1 - \boldsymbol{e}_1]$, and the alignment between $(-\boldsymbol{\tau})_2$ and $\boldsymbol{e}_2$, $\zeta[(-\boldsymbol{\tau})_2 - \boldsymbol{e}_2^P]$.

angle between the eigenvectors $(-\boldsymbol{\tau})_1$ and $\boldsymbol{e}_1$ obtained in the present study was $\approx 42^\circ$ for the $\alpha\beta\gamma - \alpha\beta\gamma$ configuration, and the most probable alignment between the eigenvectors $(-\boldsymbol{\tau})_2$ and $\boldsymbol{e}_1$ was $\approx 42^\circ$ for the $\alpha\beta\gamma - \beta\alpha\gamma$ configuration. These angles are larger than the angles reported in Tao *et al.* (2000) (34°) and in Tao *et al.* (2002) (32°).

This difference in the alignment angle may be attributed to the difference in the Reynolds number ($R_\lambda = 87.6$ in the present study and $R_\lambda = 260$ in Tao *et al.* (2002)), the difference in the filter function (the Gaussian function in the present study and the low-pass box filter function in Tao *et al.* (2002)), and the difference in the flow field (the homogeneous isotropic turbulent flow in the present study and the flow in the core region of a square duct in Tao *et al.* (2002), i.e. the presence of weak mean shear in the duct flow). We note that the most probable angle between the eigenvectors $(-\boldsymbol{\tau})_1$ and $\boldsymbol{e}_1$ which was derived using the DNS data at $R_\lambda = 93$ shown in Tao *et al.* (2002) appears to be $\cos\theta[(-\boldsymbol{\tau})_1 - \boldsymbol{e}_1] \approx 0.8$ (i.e. $\theta[(-\boldsymbol{\tau})_1 - \boldsymbol{e}_1] \approx 37^\circ$), which is slightly larger than the angle obtained using the experimental data. However, it was found that this angle is also dependent on the truncation of the DNS data. When the DNS data were truncated to 32^3 grid points ($\Delta/\eta = 24.4$, $\overline{\Delta}/\eta = 48.8$), the most probable alignment between $(-\boldsymbol{\tau})_3$ and $\boldsymbol{e}_3$ was $\cos\theta[(-\boldsymbol{\tau})_3 - \boldsymbol{e}_3] = 0.8$ (i.e. $\theta[(-\boldsymbol{\tau})_3 - \boldsymbol{e}_3] \approx 37^\circ$)

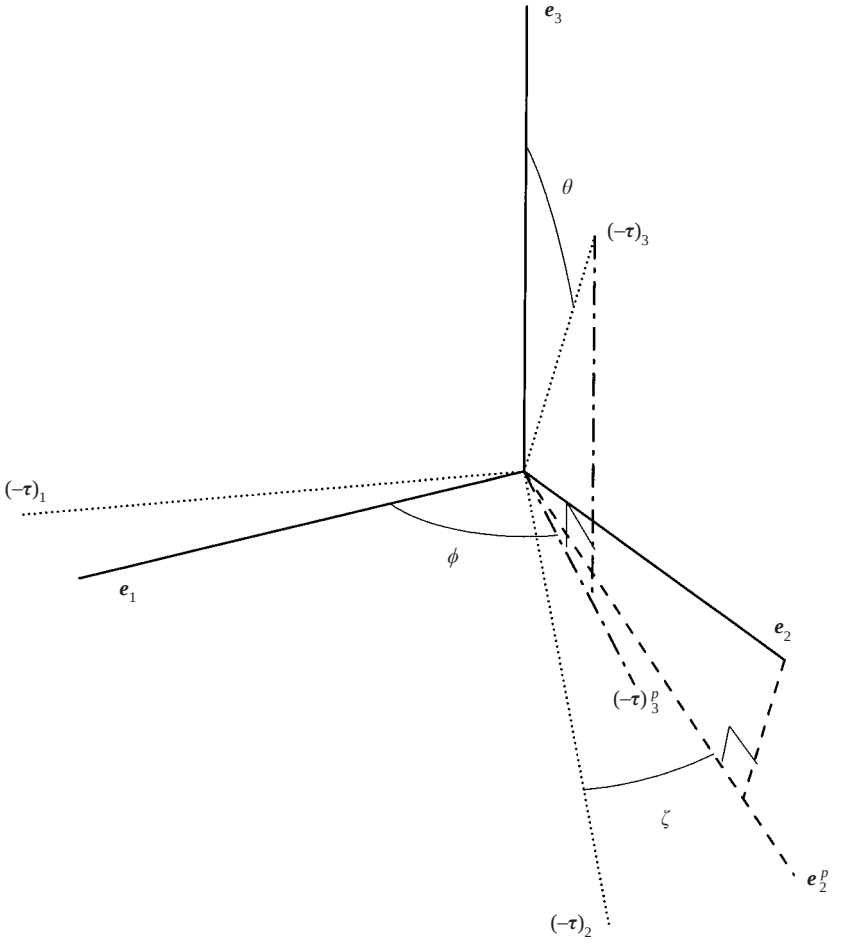

FIGURE 2. Perspective sketch for definition of angles θ, ζ, ϕ used for the p.d.f.s. The example is shown for $[(-\boldsymbol{\tau})_3 - \boldsymbol{e}_3]$ (angle between $(-\boldsymbol{\tau})_3$ and $\boldsymbol{e}_3$), and $\zeta[(-\boldsymbol{\tau})_2 - \boldsymbol{e}_2^P]$ (angle between $(-\boldsymbol{\tau})_2$ and $\boldsymbol{e}_2^P$ on the $((-\boldsymbol{\tau})_2, (-\boldsymbol{\tau})_1)$-plane), $\boldsymbol{e}_2^P$ is the projection of $\boldsymbol{e}_2$ on this plane), and $\phi[(-\boldsymbol{\tau})_3^P - \boldsymbol{e}_1]$ (angle between $\boldsymbol{e}_1$ and $(-\boldsymbol{\tau})_3^P$ on the $(\boldsymbol{e}_1, \boldsymbol{e}_2)$-plane), $(-\boldsymbol{\tau})_3^P$ is the projection of $(-\boldsymbol{\tau})_3$ on this plane).

(figure not shown), which is closer to the values reported in Tao *et al.* (2000) and Tao *et al.* (2002). This point will be discussed in § 4.

Figure 3(*a*) shows the p.d.f. of the alignment between the vorticity vector $\boldsymbol{\omega}$ and the strain-rate eigenvector $\boldsymbol{e}_i$, $\cos\theta[\boldsymbol{\omega} - \boldsymbol{e}_i]$ $(i = 1, 2, 3)$, where $\boldsymbol{\omega} = (\overline{\omega}_i)$, $\overline{\omega}_i = \varepsilon_{ilm}(\partial \overline{u}_m / \partial x_l)$, ε_{ilm} is the alternating tensor. As was shown in Ashurst *et al.* (1987), Vincent & Meneguzzi (1994) and Tao *et al.* (2002) (and the references therein), the most probable state is that the eigenvector $\boldsymbol{e}_2$ for the intermediate eigenvalue, σ_2, is aligned with the vorticity vector, $\boldsymbol{\omega}$, and the eigenvector $\boldsymbol{e}_3$ for the smallest eigenvalue, σ_3, is perpendicular to the vorticity vector. This preferential alignment of the eigenvector $\boldsymbol{e}_2$ and $\boldsymbol{\omega}$ can be explained using a Burgers vortex tube and layer models (Batchelor 1967) as was shown in Jiménez (1992), Andreotti (1997), Nomura & Post (1998) and Horiuti (2001). When the circulation around the tube and the strain along the layer are weak, $\boldsymbol{e}_1$ is parallel to $\boldsymbol{\omega}$, but when they are strong, the crossover of the eigenvalues

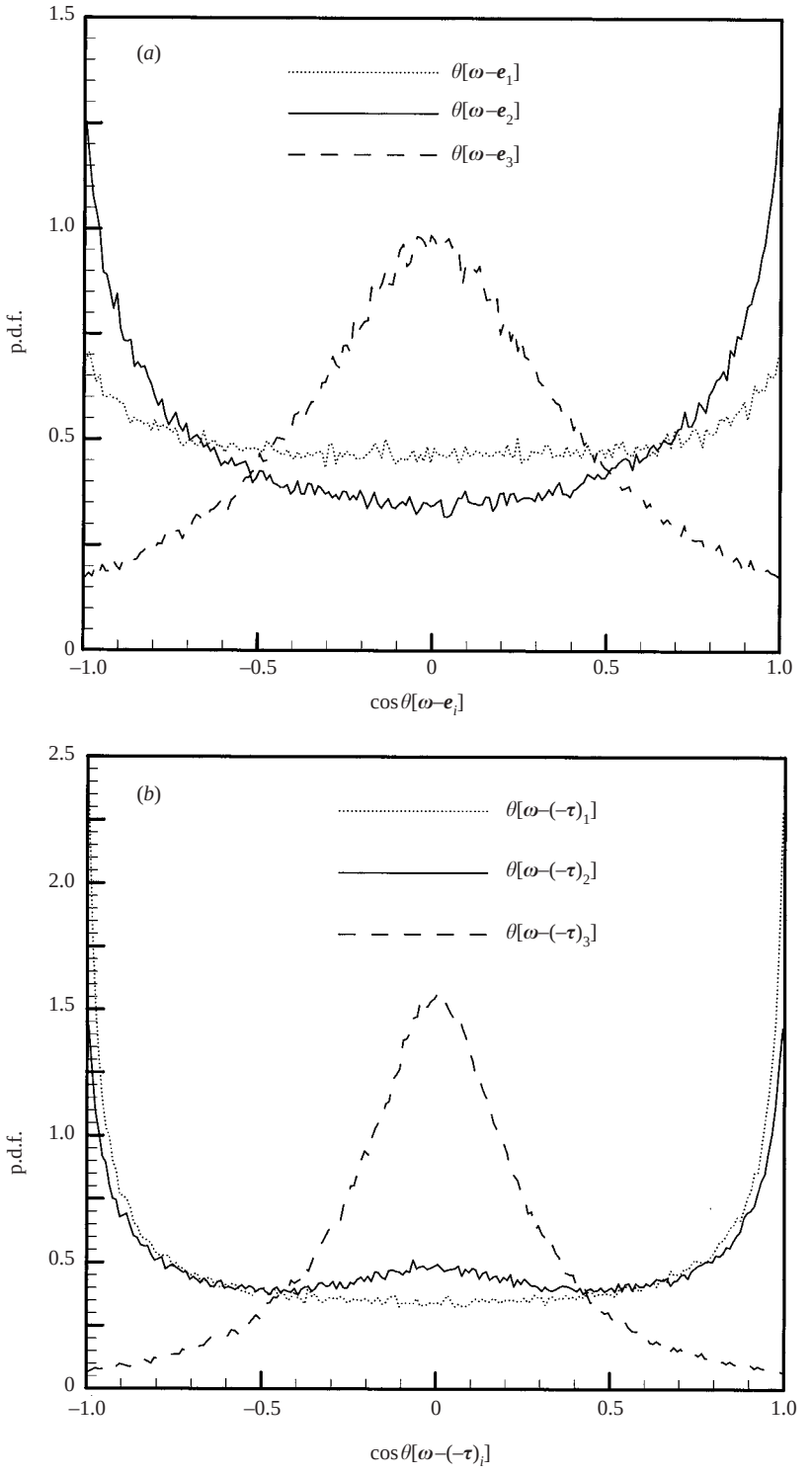

FIGURE 3. Distribution of p.d.f. for the alignment: (*a*) between the vorticity vector and the strain-rate eigenvectors, $\cos\theta[\boldsymbol{\omega}-\boldsymbol{e}_i]$ ($i = 1, 2, 3$), and (*b*) between the vorticity vector and the stress eigenvectors, $\cos\theta[\boldsymbol{\omega}-\boldsymbol{\tau}_i]$ ($i = 1, 2, 3$).

takes place along the radial axis of the tube and along the axis perpendicular to the layer, and $\boldsymbol{e}_2$ is parallel to $\boldsymbol{\omega}$.

Figure 3(b) shows the p.d.f. of the alignment between the vorticity vector $\boldsymbol{\omega}$ and the SGS stress tensor eigenvector, $(-\boldsymbol{\tau})_i$ $(i = 1, 2, 3)$, $\cos\theta[\boldsymbol{\omega} - (-\boldsymbol{\tau})_i]$ $(i = 1, 2, 3)$. The most probable state is that the eigenvector $(-\boldsymbol{\tau})_1$ for the most contracting stress eigenvalue, $(-\tau)_1$, is aligned with the vorticity vector, and the eigenvector $(-\boldsymbol{\tau})_3$ for the most extensive stress eigenvalue, $(-\tau)_3$, is perpendicular to the vorticity vector.

As a result, among the strain-rate eigenvectors, $\boldsymbol{e}_2$ is preferentially aligned with the vorticity vector, whereas, among the stress eigenvectors, $(-\boldsymbol{\tau})_1$ is preferentially aligned with the vorticity vector. The probability of occurrence of alignment of the intermediate stress eigenvector, $(-\boldsymbol{\tau})_2$, with the vorticity vector, however, is not negligibly small. Therefore, appearance of the $\alpha\beta\gamma - \alpha\beta\gamma$ configuration or the $\alpha\beta\gamma - \beta\alpha\gamma$ configuration depends on the degree of alignment of the strain-rate and stress eigenvectors with the vorticity vector, e.g. when $(-\boldsymbol{\tau})_1$ is aligned with $\boldsymbol{\omega}$, the $\alpha\beta\gamma - \beta\alpha\gamma$ configuration preferentially arises, while when $(-\boldsymbol{\tau})_2$ is aligned with $\boldsymbol{\omega}$, the $\alpha\beta\gamma - \alpha\beta\gamma$ configuration preferentially arises.

To prevent the appearance of this bimodal behaviour of alignment, we adopted an alternative reordering of the eigenvalues and corresponding eigenvectors. In the present study, the eigenvalues σ_i $(i = 1.2.3)$ were reordered so that the eigenvalue, the eigenvector of which is maximally aligned with the vorticity vector, $\boldsymbol{\omega}$, is chosen as σ_z, the largest remaining eigenvalue, as σ_+, and the smallest one, as σ_-. The corresponding eigenvectors for eigenvalues, $\sigma_z, \sigma_+, \sigma_-$, were denoted as $\boldsymbol{e}_z, \boldsymbol{e}_+, \boldsymbol{e}_-$, respectively (Andreotti 1997; Horiuti 2001). When this reordering was complete, the intermediate eigenvector $\boldsymbol{e}_2$ was preferentially reordered as $\boldsymbol{e}_z$, and this ordering took place on $\approx 48\%$ of the grid points, whereas when the stress eigenvalues, $(-\tau)_i$, were reordered, the eigenvector $(-\boldsymbol{\tau})_1$ was preferentially reordered as $(-\boldsymbol{\tau})_z$, and this ordering took place on $\approx 50\%$ of the grid points.

Figure 4(a) shows the joint p.d.f. of the alignment between the (reordered) stress eigenvector $(-\boldsymbol{\tau})_z$ and the (reordered) strain-rate eigenvector $\boldsymbol{e}_z$, $\cos\theta[(-\boldsymbol{\tau})_z - \boldsymbol{e}_z]$, and alignment between $(-\boldsymbol{\tau})_+$ and $\boldsymbol{e}_+$, $\zeta[(-\boldsymbol{\tau})_+ - \boldsymbol{e}_+^P]$. $\boldsymbol{e}_+^P$ is the projection of $\boldsymbol{e}_+$ on the $((-\boldsymbol{\tau})_+, (-\boldsymbol{\tau})_-)$-plane. The most probable state is that of $\theta[(-\boldsymbol{\tau})_z - \boldsymbol{e}_z] \approx 0$ and $\zeta[(-\boldsymbol{\tau})_+ - \boldsymbol{e}_+^P] \approx 0$. The bimodal behaviour of the alignment observed in figure 1 was eliminated, and the eigenvector $(-\boldsymbol{\tau})_z$ is preferentially aligned with $\boldsymbol{e}_z$ by definition. Figure 4(b) shows the joint p.d.f. of the alignment between $(-\boldsymbol{\tau})_-$ and $\boldsymbol{e}_-$, $\cos\theta[(-\boldsymbol{\tau})_- - \boldsymbol{e}_-]$, and alignment between $(-\boldsymbol{\tau})_z$ and $\boldsymbol{e}_z$, $\zeta[(-\boldsymbol{\tau})_z - \boldsymbol{e}_z^P]$. The most probable state is that of $\theta[(-\boldsymbol{\tau})_- - \boldsymbol{e}_-] \approx 42^\circ$ and $\zeta[(-\boldsymbol{\tau})_z - \boldsymbol{e}_z^P] \approx 0$. Shown in figure 5 are the alignment between the stress eigenvector $(-\boldsymbol{\tau})_z$ and the strain-rate eigenvector $\boldsymbol{e}_z$, $\cos\theta[(-\boldsymbol{\tau})_z - \boldsymbol{e}_z]$, the alignment between the eigenvectors $(-\boldsymbol{\tau})_+$ and $\boldsymbol{e}_+$, $\cos\theta[(-\boldsymbol{\tau})_+ - \boldsymbol{e}_+]$, and the alignment between the eigenvectors $(-\boldsymbol{\tau})_-$ and $\boldsymbol{e}_-$, $\cos\theta[(-\boldsymbol{\tau})_- - \boldsymbol{e}_-]$. It can be seen in figure 5 that the eigenvectors $((-\boldsymbol{\tau})_+, \boldsymbol{e}_+)$ and $((-\boldsymbol{\tau})_-, \boldsymbol{e}_-)$ have a strongly preferred relative orientation of $\theta[(-\boldsymbol{\tau})_\pm - \boldsymbol{e}_\pm] \approx 42^\circ$.

Using figures 4 and 5, we determined the most probable configuration of alignment of the eigenvectors $\boldsymbol{e}_z, \boldsymbol{e}_+, \boldsymbol{e}_-$ and $(-\boldsymbol{\tau})_z, (-\boldsymbol{\tau})_+, (-\boldsymbol{\tau})_-$ as that sketched in figure 6(a), which is similar to the configuration obtained in Tao *et al.* (2002), but the appearance of the bimodal behaviour has been eliminated.

In Tao *et al.* (2002), to investigate the alignment trends, a series of conditional samplings based on the magnitudes of the SGS production term, strain rate, stress, strain state parameter, and vorticity was performed. It was shown that the relative alignments are substantially affected by these parameters. When the entire field is decomposed based on the magnitudes of the strain rate and the vorticity, the structure

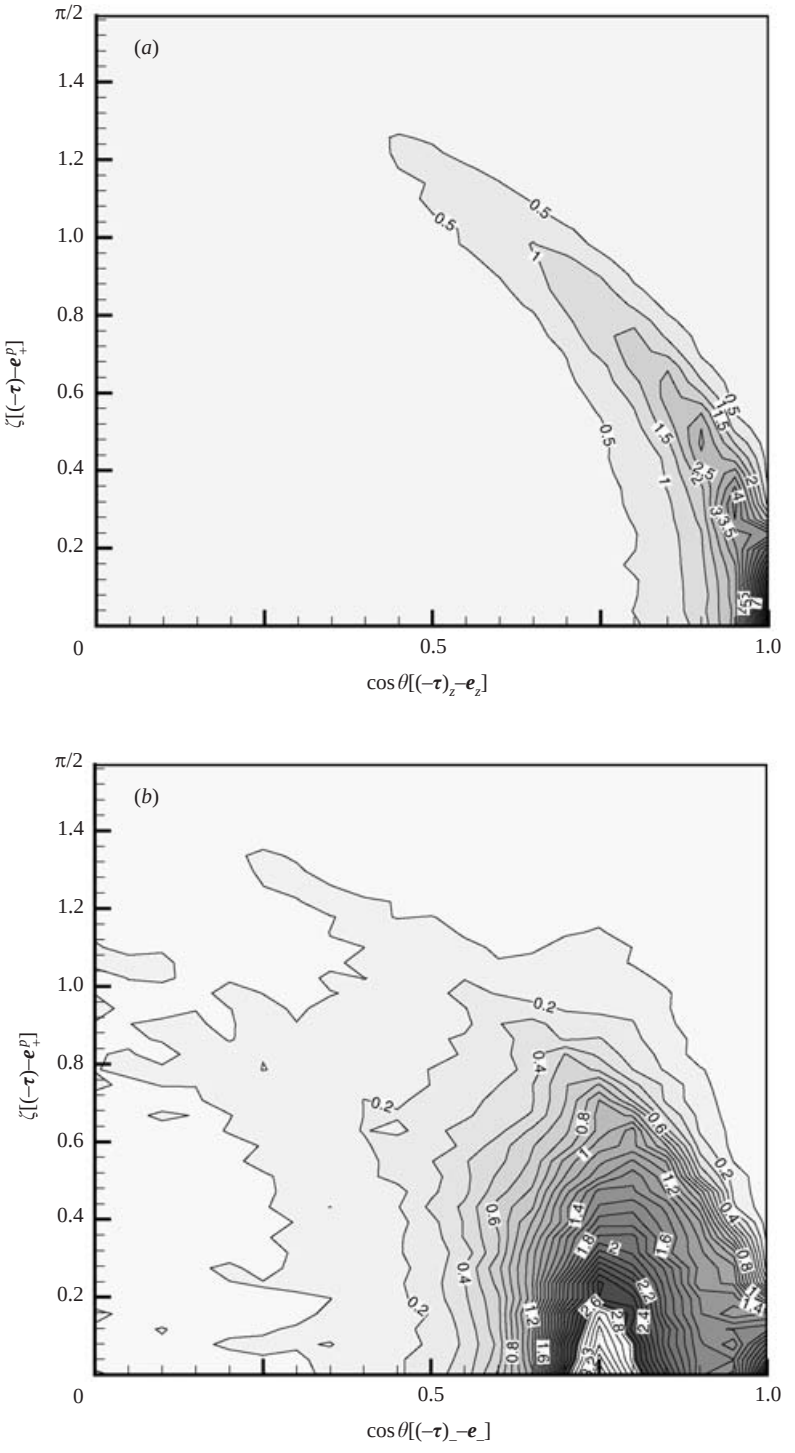

FIGURE 4. Joint p.d.f. of the alignment between the reordered strain-rate and SGS stress eigenvectors: (*a*) $\cos\theta[(-\boldsymbol{\tau})_z - \boldsymbol{e}_z]$ versus $\zeta[(-\boldsymbol{\tau})_+ - \boldsymbol{e}_+^P]$, (*b*) $\cos\theta[(-\boldsymbol{\tau})_- - \boldsymbol{e}_-]$ versus $\zeta[(-\boldsymbol{\tau})_z - \boldsymbol{e}_z^P]$.

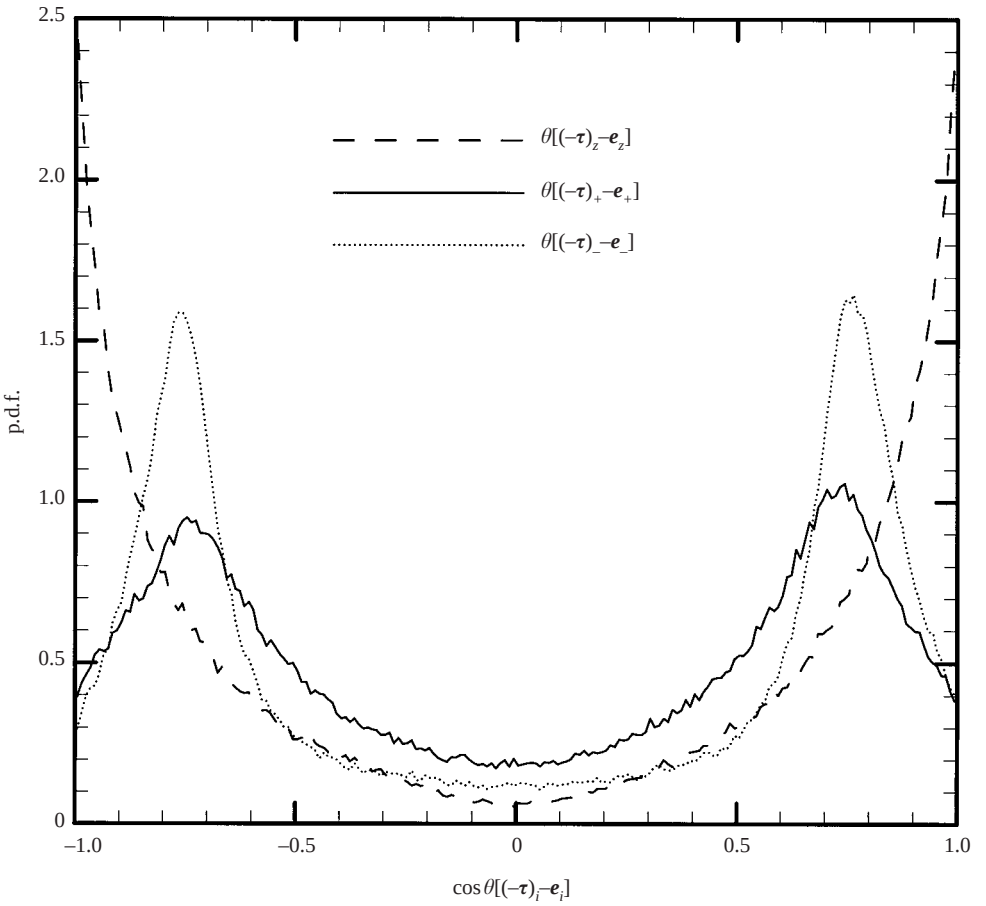

FIGURE 5. Distribution of p.d.f. for the alignment between the strain-rate eigenvectors, $\boldsymbol{e}_i$, and the SGS stress eigenvectors, $(-\boldsymbol{\tau})_i$, $\cos\theta[(-\boldsymbol{\tau})_i - \boldsymbol{e}_i]$ $(i = z, +, -)$.

of a region in which strain rate is dominant is similar to that of a cylindrical sheet around the core of a Burgers vortex tube (denoted in the following as a curved sheet), and a vorticity-dominated region is similar to a core region of a Burgers vortex tube (tube core). We note that there exists another region in which the magnitudes of vorticity and strain rate are comparable and large, and this region generally forms a sheet-like structure which is similar to a Burgers vortex layer (flat sheet). The curved sheet can be effectively identified by imposing the condition on the two reordered eigenvalues of the λ_2 method (Jeong & Hussain 1995), $\lambda_\pm$, as $\lambda_+ \geqslant \lambda_- > 0$, while the flat sheet can be identified as $\lambda_+ \geqslant 0 \geqslant \lambda_-$, and the tube core as $0 > \lambda_+ \geqslant \lambda_-$ (Horiuti 2001). In the present study, we decompose the entire turbulence field into these three regions using the above classification method.

As in Tao *et al.* (2002), it was found that the relative alignment of the strain-rate and stress eigenvectors is dependent on the decomposition of the entire field in the present study. In figure 7, the distributions of the p.d.f.s for $\cos\theta[(-\boldsymbol{\tau})_- - \boldsymbol{e}_-]$ which are decomposed into those in the curved-sheet, flat-sheet and tube-core regions are shown. It can be seen that the most preferred angle of the alignment between $(-\boldsymbol{\tau})_-$ and $\boldsymbol{e}_-$ is the smallest one in the curved-sheet region ($\cos\theta[(-\boldsymbol{\tau})_- - \boldsymbol{e}_-] \approx 0.83$, i.e. $\theta[(-\boldsymbol{\tau})_- - \boldsymbol{e}_-] \approx 33^\circ$), the largest one in the tube-core region ($\cos\theta[(-\boldsymbol{\tau})_- - \boldsymbol{e}_-] \approx 0.73$,

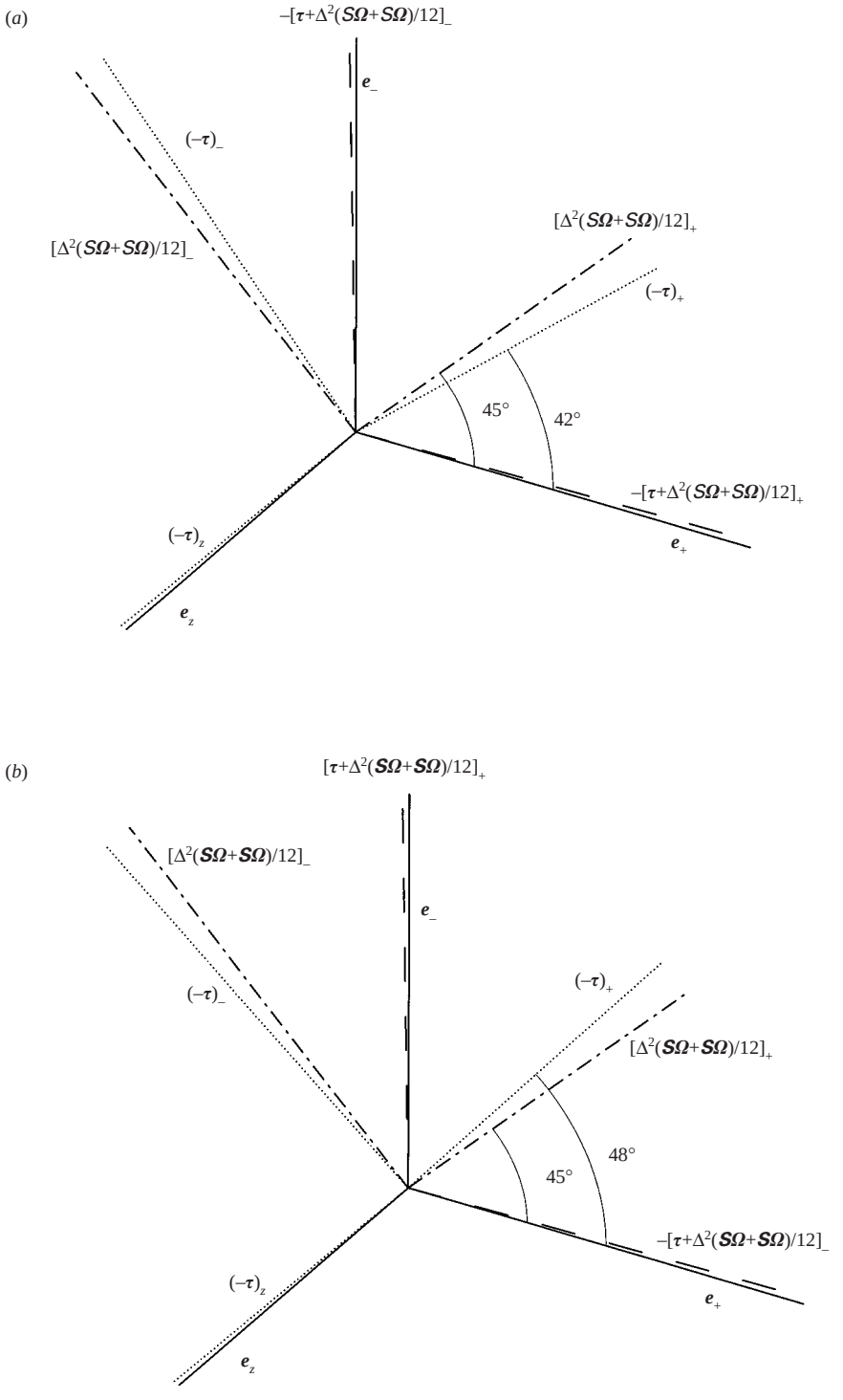

FIGURE 6. Perspective sketch of the most probable alignment configuration between the eigen-directions of the strain-rate tensor and the SGS stress tensor: (*a*) identified for the whole region, and (*b*) identified by conditionally sampling for the backward scatter events ($P < 0$).

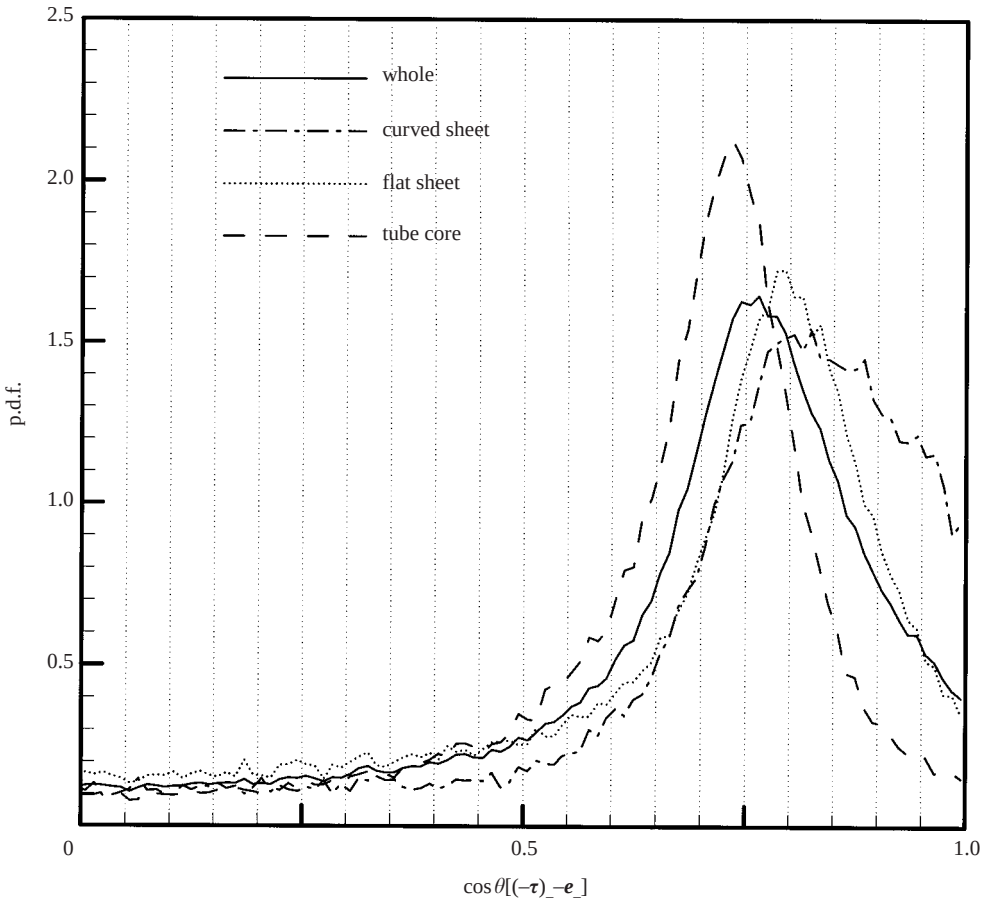

FIGURE 7. Distributions of p.d.f. for the alignment between the stress eigenvector, $(-\boldsymbol{\tau})_-$, and the strain-rate eigenvector, $\boldsymbol{e}_-$, $\cos\theta[(-\boldsymbol{\tau})_- - \boldsymbol{e}_-]$, which are decomposed into the curved sheet, flat sheet and tube core regions.

i.e. $\theta[(-\boldsymbol{\tau})_- - \boldsymbol{e}_-] \approx 43^\circ$), and the intermediate one in the flat-sheet region ($\cos\theta[(-\boldsymbol{\tau})_- - \boldsymbol{e}_-] \approx 0.79$, i.e. $\theta[(-\boldsymbol{\tau})_- - \boldsymbol{e}_-] \approx 38^\circ$).

Figure 8 shows the joint p.d.f. of the alignment between the stress eigenvector $(-\boldsymbol{\tau})_-$ and the strain-rate eigenvector $\boldsymbol{e}_-$, $\cos\theta[(-\boldsymbol{\tau})_- - \boldsymbol{e}_-]$, and alignment between $(-\boldsymbol{\tau})_z$ and $\boldsymbol{e}_z$, $\zeta[(-\boldsymbol{\tau})_z - \boldsymbol{e}_z^P]$, which was conditionally sampled in the flat-sheet region. Different from the joint p.d.f. for $\cos\theta[(-\boldsymbol{\tau})_- - \boldsymbol{e}_-]$ versus $\zeta[(-\boldsymbol{\tau})_z - \boldsymbol{e}_z^P]$ sampled in the entire region shown in figure 4(*b*), the peak of the p.d.f. is located at $\cos\theta[(-\boldsymbol{\tau})_- - \boldsymbol{e}_-] \approx 0.8$ (i.e. $\theta[(-\boldsymbol{\tau})_- - \boldsymbol{e}_-] \approx 38^\circ$) and $\zeta[(-\boldsymbol{\tau})_z - \boldsymbol{e}_z^P] \approx 17^\circ$. This peak emerged selectively in the flat-sheet region. The weak peak in figure 4(*a*) discernible at $\cos\theta[(-\boldsymbol{\tau})_z - \boldsymbol{e}_z] \approx 0.95$ (i.e. $\theta[(-\boldsymbol{\tau})_z - \boldsymbol{e}_z] \approx 18^\circ$) and $\zeta[(-\boldsymbol{\tau})_+ - \boldsymbol{e}_+^P] \approx 18^\circ$ corresponds to this peak. These results indicate that the alignment configuration in the flat-sheet region is somewhat different from those in the tube-core and curved-sheet regions. In fact, when the strain state acting on each region was interpreted using the strain parameter, $s^*(=-3\sqrt{6}\sigma_1\sigma_2\sigma_3/(\sigma_1^2+\sigma_2^2+\sigma_3^2)^{3/2})$ (Lund & Rogers 1994), the strain state acting on the flat-sheet region was different from those acting on the tube-core and curved-sheet regions. The distributions of the p.d.f.s for s^* in these three regions (figure not shown) were similar to those shown in figure 7 of Horiuti (2001), and s^*

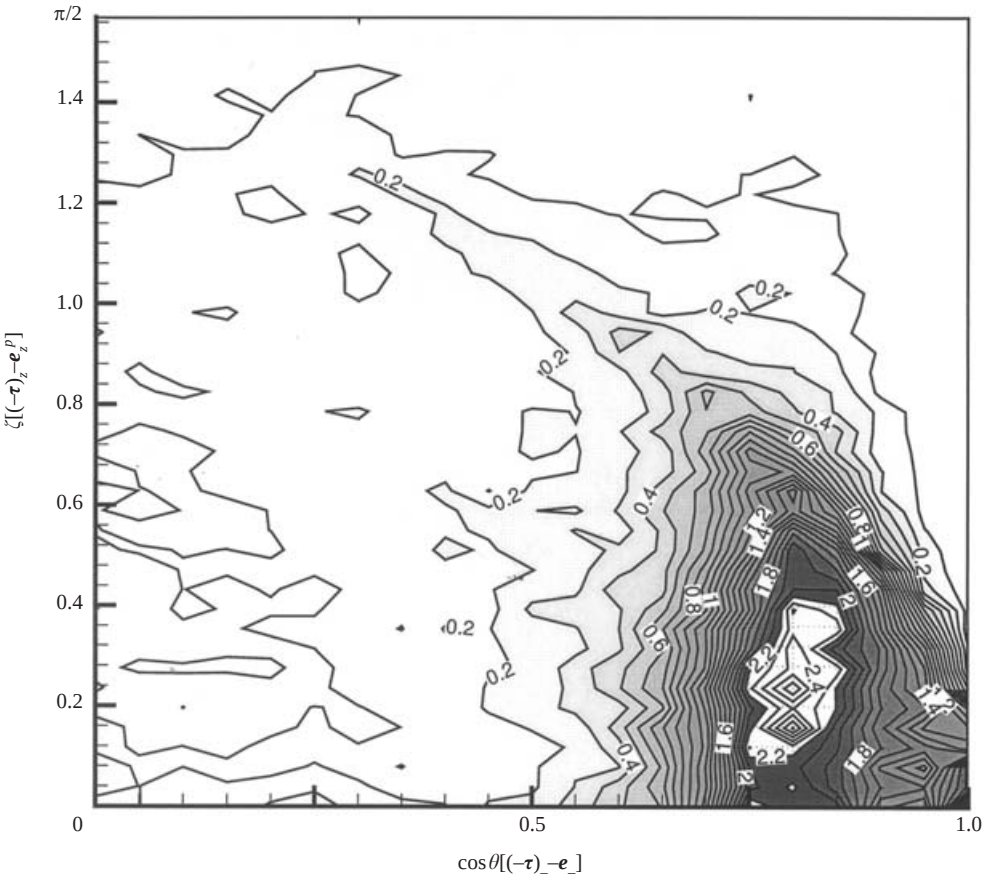

FIGURE 8. Joint p.d.f. of the alignment between the stress eigenvector $(-\boldsymbol{\tau})_-$ and the strain-rate eigenvector $\boldsymbol{e}_-$, $\cos\theta[(-\boldsymbol{\tau})_- - \boldsymbol{e}_-]$, and alignment between $(-\boldsymbol{\tau})_z$ and $\boldsymbol{e}_z$, $\zeta[(-\boldsymbol{\tau})_z - \boldsymbol{e}_z^P]$, which was conditionally sampled in the flat-sheet region.

showed a weak maximum near $s^* = 0.9$ in the flat-sheet region. Using figures 8 and 4(a), we determined the most probable configuration of alignment in the flat-sheet region to be that sketched in figure 9. Note that $(-\boldsymbol{\tau})_z$ is on the $(\boldsymbol{e}_z - \boldsymbol{e}_+)$-plane in figure 9. The distributions of the p.d.f.s for $\cos\theta[(-\boldsymbol{\tau})_- - \boldsymbol{e}_-]$ versus $\zeta[(-\boldsymbol{\tau})_z - \boldsymbol{e}_z^P]$ sampled in the tube-core and curved-sheet regions were similar to that shown in figure 4(b), and thus the most probable alignment configuration in the tube-core and curved-sheet regions was that shown in figure 6(a).

3. Decomposition of the SGS stress tensor

To identify the specific term which causes the non-alignment of the eigenvectors for the SGS stress and strain-rate tensors described in the previous section, we decompose the SGS stress tensor, τ_{ij}, using the nonlinear model, (1.6), as,

$$\tau_{ij} \simeq \frac{\overline{\Delta}^2}{12}\frac{\partial \overline{u}_i}{\partial x_k}\frac{\partial \overline{u}_j}{\partial x_k} = \frac{\overline{\Delta}^2}{12}\{(\overline{S}_{ik}\overline{S}_{kj} - \overline{\Omega}_{ik}\overline{\Omega}_{kj}) - (\overline{S}_{ik}\overline{\Omega}_{kj} + \overline{S}_{jk}\overline{\Omega}_{ki})\}, \qquad (3.1)$$

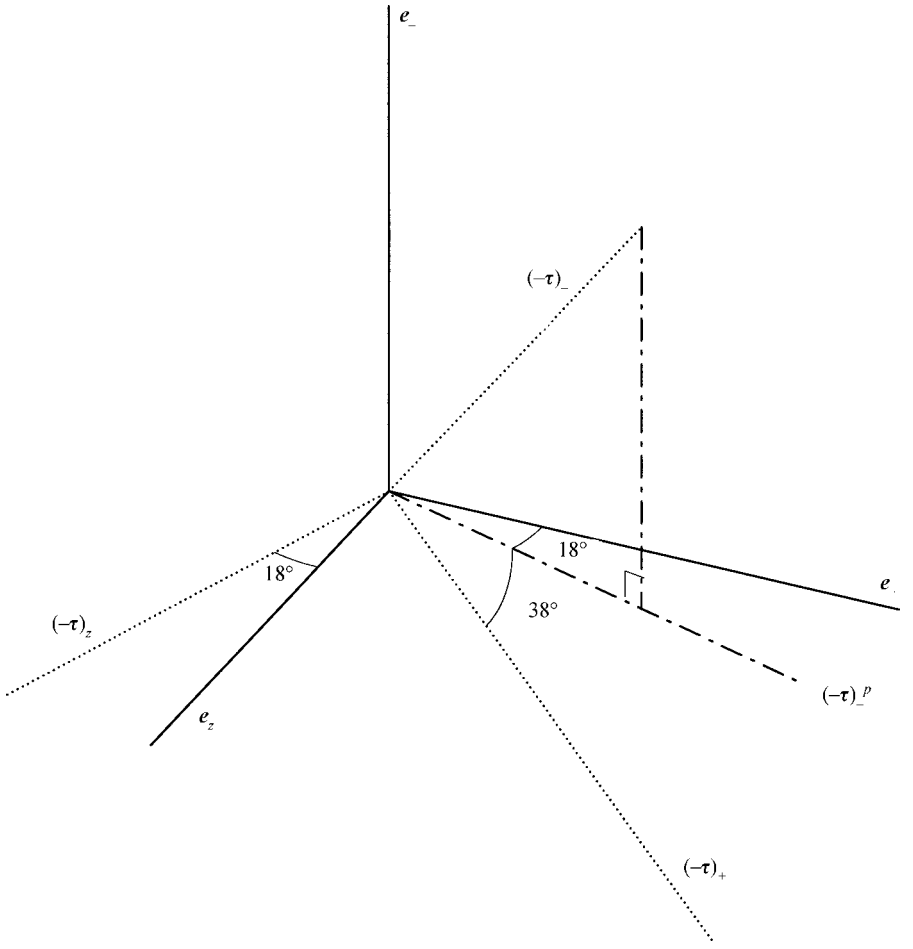

FIGURE 9. Perspective sketch of the most probable alignment configuration between the eigen-directions of the strain-rate tensor and the SGS stress tensor, which was conditionally sampled in the flat-sheet region.

where $\overline{\Omega}_{ij}(=(\partial\overline{u}_i/\partial x_j - \partial\overline{u}_j/\partial x_i)/2)$ is the grid-scale vorticity tensor. For a general form of the nonlinear model, see the Appendix. We examine the alignment of eigenvectors for each term in (3.1) with the strain-rate eigenvectors. Figures 10(a) and 10(b), respectively, show the alignment between $\boldsymbol{e}_i$ and the eigenvectors for the $-\overline{\Delta}^2(\overline{S}_{ik}\overline{S}_{kj}-\overline{\Omega}_{ik}\overline{\Omega}_{kj})/12$ term, and the alignment between $\boldsymbol{e}_i$ and the eigenvectors for the $\overline{\Delta}^2(\overline{S}_{ik}\overline{\Omega}_{kj}+\overline{S}_{jk}\overline{\Omega}_{ki})/12$ term. The eigenvectors for the $-\overline{\Delta}^2(\overline{S}_{ik}\overline{S}_{kj}-\overline{\Omega}_{ik}\overline{\Omega}_{kj})/12$ term, $-[\overline{\Delta}^2(\boldsymbol{SS}-\boldsymbol{\Omega\Omega})/12]_i$, are highly aligned with the strain-rate eigenvectors, whereas positive and negative components of eigenvectors for the $\overline{\Delta}^2(\overline{S}_{ik}\overline{\Omega}_{kj}+\overline{S}_{jk}\overline{\Omega}_{ki})/12$ term, $[\overline{\Delta}^2(\boldsymbol{S\Omega}+\boldsymbol{S\Omega})/12]_{\pm}$, make preferential angles of 45° with $\boldsymbol{e}_{\pm}$, respectively.

This angle (45°) can be derived by considering the eigenvalues for the matrix, $\boldsymbol{S\Omega}+\boldsymbol{S\Omega}$, the elements of which consist of the $(\overline{S}_{ik}\overline{\Omega}_{kj}+\overline{S}_{jk}\overline{\Omega}_{ki})$ terms. The elements of $\boldsymbol{S}$ and $\boldsymbol{\Omega}$ are, respectively, $\overline{S}_{ij}$ and $\overline{\Omega}_{ij}$. The matrix $\boldsymbol{S\Omega}+\boldsymbol{S\Omega}$ on the basis of the principal strain eigenvectors, $\boldsymbol{e}_+, \boldsymbol{e}_-, \boldsymbol{e}_z$, $\boldsymbol{E}^{\boldsymbol{T}}(\boldsymbol{S\Omega}+\boldsymbol{S\Omega})\boldsymbol{E}$, can be

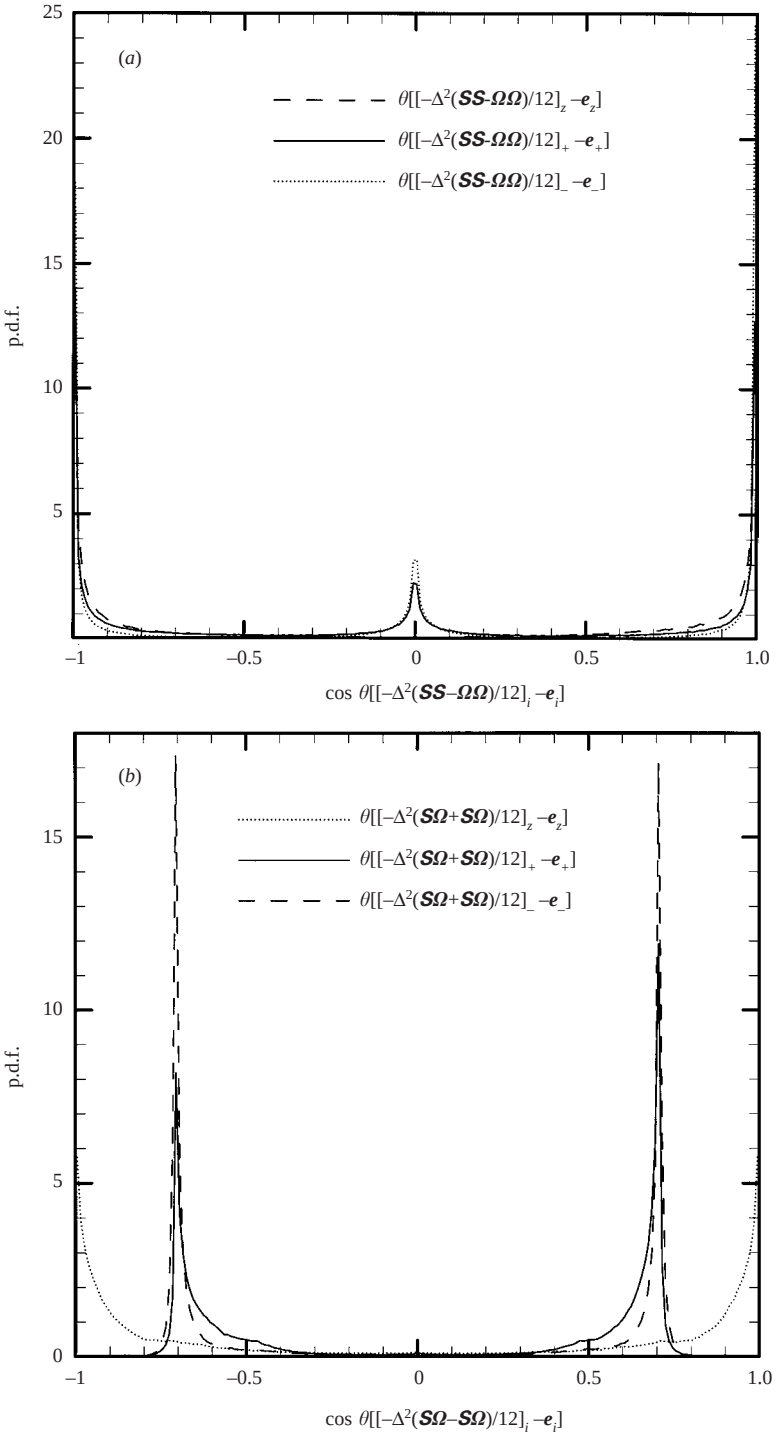

FIGURE 10. Distribution of p.d.f. for the alignment: (*a*) between the eigenvectors for the $-\overline{\Delta}^2(\overline{S}_{ik}\overline{S}_{kj} - \overline{\Omega}_{ik}\overline{\Omega}_{kj})/12$ term, and the strain-rate eigenvectors, $\boldsymbol{e}_i$, $\cos\theta[-[\overline{\Delta}^2(\boldsymbol{SS} - \boldsymbol{\Omega\Omega})/12]_i - \boldsymbol{e}_i]$ $(i = z, +, -)$, and (*b*) between the eigenvectors for the $\overline{\Delta}^2(\overline{S}_{ik}\overline{\Omega}_{kj} + \overline{S}_{jk}\overline{\Omega}_{ki})/12$ term, and $\boldsymbol{e}_i$, $\cos\theta[[\overline{\Delta}^2(\boldsymbol{S\Omega} + \boldsymbol{S\Omega})/12]_i - \boldsymbol{e}_i]$ $(i = z, +, -)$.

obtained as

$$\boldsymbol{L} = \begin{pmatrix} 0 & -\frac{1}{2}(\sigma_+ - \sigma_-)\overline{\omega}_z & \frac{1}{2}(\sigma_+ - \sigma_z)\overline{\omega}_- \\ -\frac{1}{2}(\sigma_+ - \sigma_-)\overline{\omega}_z & 0 & -\frac{1}{2}(\sigma_- - \sigma_z)\overline{\omega}_+ \\ \frac{1}{2}(\sigma_+ - \sigma_z)\overline{\omega}_- & -\frac{1}{2}(\sigma_- - \sigma_z)\overline{\omega}_+ & 0 \end{pmatrix}.$$

The matrices, $\boldsymbol{E}$ and $\boldsymbol{E}^{\boldsymbol{T}}$, are orthogonal matrices whose rows and columns, respectively, are $\boldsymbol{e}_+, \boldsymbol{e}_-, \boldsymbol{e}_z$ (Nomura & Post 1998). $\overline{\omega}_+, \overline{\omega}_-, \overline{\omega}_z$ are the vorticity components projected onto the basis of the principal strain eigenvectors, $\boldsymbol{\omega}\cdot\boldsymbol{e}_+, \boldsymbol{\omega}\cdot\boldsymbol{e}_-, \boldsymbol{\omega}\cdot\boldsymbol{e}_z$, respectively. Note that the trace of the $(\overline{S}_{ik}\overline{\Omega}_{kj} + \overline{S}_{jk}\overline{\Omega}_{ki})$ terms is equal to zero, thus the trace of the matrix $\boldsymbol{L}$ is zero.

Because the amplitude of $\overline{\omega}_z$ is predominantly larger than those of $\overline{\omega}_+$ and $\overline{\omega}_-$, the matrix $\boldsymbol{L}$ can be approximated as

$$\boldsymbol{L}' = \begin{pmatrix} 0 & -\frac{1}{2}(\sigma_+ - \sigma_-)\overline{\omega}_z & 0 \\ -\frac{1}{2}(\sigma_+ - \sigma_-)\overline{\omega}_z & 0 & 0 \\ 0 & 0 & 0 \end{pmatrix}.$$

It can be readily seen that the eigenvalue of $\boldsymbol{L}'$ in the stretching direction ($\boldsymbol{e}_z$) is zero. The remaining two eigenvalues are

$$\tfrac{1}{2}(\sigma_+ - \sigma_-)\overline{\omega}_z, -\tfrac{1}{2}(\sigma_+ - \sigma_-)\overline{\omega}_z, \tag{3.2}$$

and their eigenvectors make angles of 45° with the strain-rate eigenvectors, $\boldsymbol{e}_+, \boldsymbol{e}_-$.

Similarly, the matrix, $\boldsymbol{SS} - \boldsymbol{\Omega\Omega}$, the elements of which consist of the $(\overline{S}_{ik}\overline{S}_{kj} - \overline{\Omega}_{ik}\overline{\Omega}_{kj})$ terms on the basis of the principal strain eigenvectors, $\boldsymbol{E}^{\boldsymbol{T}}(\boldsymbol{SS} - \boldsymbol{\Omega\Omega})\boldsymbol{E}$, can be derived as

$$\boldsymbol{M} = \begin{pmatrix} \sigma_+^2 + \frac{1}{4}(\overline{\omega}_-^2 + \overline{\omega}_z^2) & \frac{1}{4}\overline{\omega}_+\overline{\omega}_- & \frac{1}{4}\overline{\omega}_+\overline{\omega}_z \\ \frac{1}{4}\overline{\omega}_-\overline{\omega}_+ & \sigma_-^2 + \frac{1}{4}(\overline{\omega}_+^2 + \overline{\omega}_z^2) & \frac{1}{4}\overline{\omega}_-\overline{\omega}_z \\ \frac{1}{4}\overline{\omega}_z\overline{\omega}_+ & \frac{1}{4}\overline{\omega}_z\overline{\omega}_- & \sigma_z^2 + \frac{1}{4}(\overline{\omega}_+^2 + \overline{\omega}_-^2) \end{pmatrix}.$$

Because the amplitudes of off-diagonal elements of matrix $\boldsymbol{M}$, $\overline{\omega}_+\overline{\omega}_-, \overline{\omega}_+\overline{\omega}_z, \overline{\omega}_-\overline{\omega}_z$, were negligibly small in the DNS data, the matrix $\boldsymbol{M}$ can be approximately rewritten as

$$\boldsymbol{M}' = \begin{pmatrix} \sigma_+^2 + \frac{1}{4}(\overline{\omega}_-^2 + \overline{\omega}_z^2) & 0 & 0 \\ 0 & \sigma_-^2 + \frac{1}{4}(\overline{\omega}_+^2 + \overline{\omega}_z^2) & 0 \\ 0 & 0 & \sigma_z^2 + \frac{1}{4}(\overline{\omega}_+^2 + \overline{\omega}_-^2) \end{pmatrix}.$$

It can be seen that the eigenvectors for the $(\overline{S}_{ik}\overline{S}_{kj} - \overline{\Omega}_{ik}\overline{\Omega}_{kj})$ term are almost parallel to the eigenvectors for the strain-rate tensor. The matrix $\boldsymbol{M}'$ constitutes the normal components of the SGS stress tensor, whereas the matrix $\boldsymbol{L}'$ constitutes the shear components of the SGS stress tensor on the basis of $\boldsymbol{e}_z, \boldsymbol{e}_+, \boldsymbol{e}_-$.

It is shown that non-alignment of eigenvectors primarily arises in the $-\overline{\Delta}^2(\overline{S}_{ik}\overline{\Omega}_{kj} + \overline{S}_{jk}\overline{\Omega}_{ki})/12$ term. Figure 11 shows the alignment of the eigenvectors for the $-(\tau_{ij} + \overline{\Delta}^2(\overline{S}_{ik}\overline{\Omega}_{kj} + \overline{S}_{jk}\overline{\Omega}_{ki})/12)$ term, $-[\boldsymbol{\tau} + \overline{\Delta}^2(\boldsymbol{S\Omega} + \boldsymbol{S\Omega})/12]_i$, and the strain-rate eigenvectors, $\cos\theta[-[\boldsymbol{\tau} + \overline{\Delta}^2(\boldsymbol{S\Omega} + \boldsymbol{S\Omega})/12]_i - \boldsymbol{e}_i]$. It can be seen that when the $-\overline{\Delta}^2(\overline{S}_{ik}\overline{\Omega}_{kj} + \overline{S}_{jk}\overline{\Omega}_{ki})/12$ term was subtracted from the τ_{ij} term, the eigenvectors for the remainder were nearly parallel to the strain-rate eigenvectors. We note that this

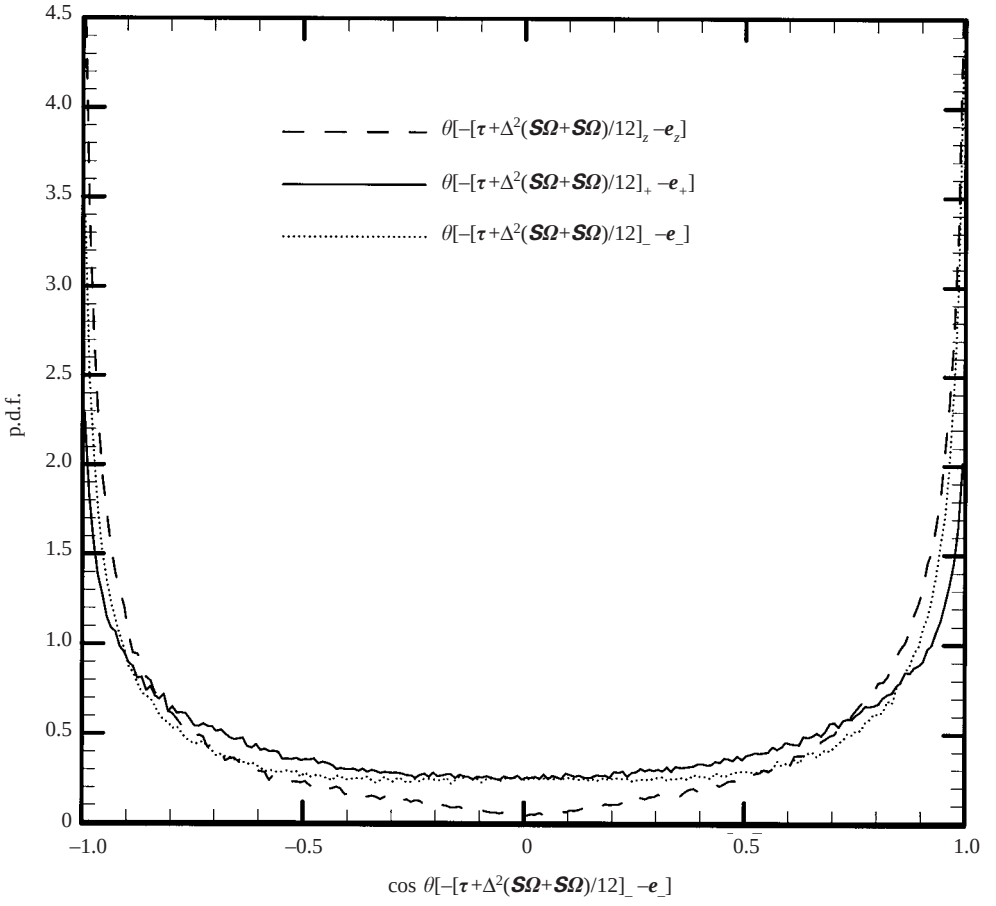

FIGURE 11. Distribution of p.d.f. for the alignment between the eigenvectors for the $-(\tau_{ij} + \overline{\Delta}^2(\overline{S}_{ik}\overline{\Omega}_{kj} + \overline{S}_{jk}\overline{\Omega}_{ki})/12)$ term and the strain-rate eigenvectors, $\boldsymbol{e}_i$, $\cos\theta[-[\boldsymbol{\tau} + \overline{\Delta}^2(\boldsymbol{S\Omega} + \boldsymbol{S\Omega})/12]_i - \boldsymbol{e}_i]$ $(i = z, +, -)$.

alignment trend was unchanged even when the DNS data were truncated to more coarse grid points (32^3) (figure not shown).

In figure 6(a), we included the sketch of the alignment configuration for the eigenvectors of the $\overline{\Delta}^2(\overline{S}_{ik}\overline{\Omega}_{kj} + \overline{S}_{jk}\overline{\Omega}_{ki})/12$ term, $[\overline{\Delta}^2(\boldsymbol{S\Omega} + \boldsymbol{S\Omega})/12]_i$, and the $-(\tau_{ij} + \overline{\Delta}^2(\overline{S}_{ik}\overline{\Omega}_{kj} + \overline{S}_{jk}\overline{\Omega}_{ki})/12)$ term, $-[\boldsymbol{\tau} + \overline{\Delta}^2(\boldsymbol{S\Omega} + \boldsymbol{S\Omega})/12]_i$. The angle which the eigenvector for the $(-\tau_{ij})$ term, $(-\boldsymbol{\tau})_+$, forms with $\boldsymbol{e}_+$, $\theta[(-\boldsymbol{\tau})_+ - \boldsymbol{e}_+]$, is intermediate between the angle $\theta[[\overline{\Delta}^2(\boldsymbol{S\Omega} + \boldsymbol{S\Omega})/12]_+ - \boldsymbol{e}_+](\approx 45^\circ)$ and the angle $\theta[-[\boldsymbol{\tau} + \overline{\Delta}^2(\boldsymbol{S\Omega} + \boldsymbol{S\Omega})/12]_+ - \boldsymbol{e}_+](\approx 0^\circ)$, i.e. $0 < \theta[(-\boldsymbol{\tau})_+ - \boldsymbol{e}_+] < 45^\circ$. Similarly, $\theta[(-\boldsymbol{\tau})_- - \boldsymbol{e}_-]$, is intermediate between the angle $\theta[[\overline{\Delta}^2(\boldsymbol{S\Omega} + \boldsymbol{S\Omega})/12]_- - \boldsymbol{e}_-]$ and the angle $\theta[-[\boldsymbol{\tau} + \overline{\Delta}^2(\boldsymbol{S\Omega} + \boldsymbol{S\Omega})/12]_- - \boldsymbol{e}_-]$.

An energy cascade between the grid scale and the SGS takes place through the SGS energy transfer term as

$$\overline{u}_i \frac{\partial \tau_{ij}}{\partial x_j} = \frac{\partial}{\partial x_j}(\overline{u}_i \tau_{ij}) - \tau_{ij}\overline{S}_{ij}, \tag{3.3}$$

which has been used to analyse the energy exchange between the grid scale and the SGS in Kerr, Domaradzki & Barbier (1996) and Langford & Moser (1999). Kerr *et al.* (1996) showed that the SGS energy transfer term contains both large forward scatter of the grid-scale energy into the SGS and backward scatter of the SGS energy into the grid scale, and the magnitude of the latter is comparable with that of the former. When the right-hand side of (3.3) is integrated in the entire computational domain, the first term vanishes. Therefore, forward and backward scatters are equally generated via the first term. Because the first term makes no contribution to the SGS energy transfer on average, and also because the first term cannot be considered on the basis of the principal strain eigenvectors, whereas the second term can be considered on this basis, we analysed the energy transfer using the second term in (3.3), P.

The second term can be written in a general form as the (generalized) SGS production term, P_{ij},

$$P_{ij} = -(\tau_{ik}\overline{S}_{kj} + \tau_{jk}\overline{S}_{ki})/2. \tag{3.4}$$

It should be noted that, in the trace of P_{ij}, i.e. the total production term $P_{ii}(= P)$, the $-\overline{\Delta}^2(\overline{S}_{ik}\overline{\Omega}_{kj} + \overline{S}_{jk}\overline{\Omega}_{ki})/12$ term vanishes (Kosović 1997), thus the $-\overline{\Delta}^2(\overline{S}_{ik}\overline{\Omega}_{kj} + \overline{S}_{jk}\overline{\Omega}_{ki})/12$ term makes no contribution to the production of the total SGS energy. This is why the low correlation between the exact τ_{ij} term and the τ_{ij} term approximated using the Smagorinsky model was markedly improved when the correlation between them was calculated on the SGS production term, P. The first term in (3.1) yields the estimate of the exact production term as

$$P \approx \overline{\Delta}^2\{-(\overline{S}_{ik}\overline{S}_{kj} - \overline{\Omega}_{ik}\overline{\Omega}_{kj})\overline{S}_{ji}\}/12. \tag{3.5}$$

The first term in (3.5),

$$-\overline{S}_{ik}\overline{S}_{kj}\overline{S}_{ji} = -3\sigma_1\sigma_2\sigma_3 = -3\sigma_z\sigma_+\sigma_-, \tag{3.6}$$

is the skewness of the grid-scale velocity gradient and is equal to the production term for the grid-scale strain rate, $\overline{S}_{ik}\overline{S}_{ki}/2$. The second term in (3.5), $\overline{\Omega}_{ik}\overline{\Omega}_{kj}\overline{S}_{ji}$, is the grid-scale vortex-stretching term and is the production term for the grid-scale enstrophy, $-\overline{\Omega}_{ik}\overline{\Omega}_{ki}/2$.

Because the eigenvectors for the $-(\tau_{ij} + \overline{\Delta}^2(\overline{S}_{ik}\overline{\Omega}_{kj} + \overline{S}_{jk}\overline{\Omega}_{ki})/12)$ term are approximately aligned with the strain-rate eigenvectors, the matrix which consists of the $-(\tau_{ij} + \overline{\Delta}^2(\overline{S}_{ik}\overline{\Omega}_{kj} + \overline{S}_{jk}\overline{\Omega}_{ki})/12)$ terms and the matrix which consists of the $\overline{S}_{ij}$ terms can be simultaneously diagonalized when the matrices are transformed on the basis of the principal strain eigenvectors. If the diagonal elements of the transformed matrices, i.e. eigenvalues of these two matrices, are close to each other, the SGS eddy-viscosity model may be adequate to approximate the τ_{ij} term, when the performance of the SGS model is evaluated based on the accuracy of its estimation of the total production term, P. The eigenvalue of the $-(\tau_{ij} + \overline{\Delta}^2(\overline{S}_{ik}\overline{\Omega}_{kj} + \overline{S}_{jk}\overline{\Omega}_{ki})/12)$ term, $-[\tau_{ij} + \overline{\Delta}^2(\overline{S}_{ik}\overline{\Omega}_{kj} + \overline{S}_{jk}\overline{\Omega}_{ki})/12]_+$ and the strain-rate eigenvalue, σ_+, however, were poorly correlated ($\rho \approx -0.085$, figure not shown). Another eigenvalue of the $-(\tau_{ij} + \overline{\Delta}^2(\overline{S}_{ik}\overline{\Omega}_{kj} + \overline{S}_{jk}\overline{\Omega}_{ki})/12)$ term, $-[\tau_{ij} + \overline{\Delta}^2(\overline{S}_{ik}\overline{\Omega}_{kj} + \overline{S}_{jk}\overline{\Omega}_{ki})/12]_-$ and the strain-rate eigenvalue, σ_- were better correlated ($\rho \approx 0.46$), but their correlation is still low. These results indicate another drawback of the (isotropic) SGS eddy-viscosity model, that is, the isotropic SGS eddy-viscosity coefficient is inadequate and the anisotropic coefficient is more desirable for approximating the τ_{ij} term.

In the generalized production term, P_{ij}, elimination of the $-\overline{\Delta}^2(\overline{S}_{ik}\overline{\Omega}_{kj}+\overline{S}_{jk}\overline{\Omega}_{ki})/12$ term does not take place. To examine whether the influence of the off-diagonal elements of the matrix, (P_{ij}), the elements of which consist of the P_{ij} terms, on the generalized production term is significant, we examined the eigenvalues for the matrix, (P_{ij}). The magnitudes of the eigenvalues of the matrix, (P_{ij}), were reduced to approximately half when the eigenvalues were calculated by subtracting the $-\overline{\Delta}^2(\overline{S}_{ik}\overline{\Omega}_{kj}+\overline{S}_{jk}\overline{\Omega}_{ki})/12$ term from the τ_{ij} term (figure not shown). This result indicates that the $-\overline{\Delta}^2(\overline{S}_{ik}\overline{\Omega}_{kj}+\overline{S}_{jk}\overline{\Omega}_{ki})/12$ term which causes non-alignment of the eigenvectors makes a noticeable contribution to the generalized production term, P_{ij}, although it makes no contribution to the trace of the P_{ij} term, implying that the off-diagonal components of the P_{ij} term are as important as the diagonal components, and should be taken into consideration for a proper SGS modelling. As was suggested in Langford & Moser (1999), the difference in the magnitudes of the eigenvalues of the matrix (P_{ij}) in which the $-\overline{\Delta}^2(\overline{S}_{ik}\overline{\Omega}_{kj}+\overline{S}_{jk}\overline{\Omega}_{ki})/12$ term was retained in the τ_{ij} term and the eigenvalues in which the $-\overline{\Delta}^2(\overline{S}_{ik}\overline{\Omega}_{kj}+\overline{S}_{jk}\overline{\Omega}_{ki})/12$ term was removed from the τ_{ij} term may become larger in turbulence with mean shear than in that without mean shear, since the shear stress does not vanish on average in a sheared turbulence.

In the dynamic Smagorinsky model (DSM) (Piomelli *et al.* 1991), the model parameter C_S was determined as $C_S=(\mathscr{L}_{ij}\mathscr{E}_{ij})/(\mathscr{E}_{ij}\mathscr{E}_{ij})$, where $\mathscr{L}_{ij}=(\widetilde{\overline{u}_i\overline{u}_j}-\tilde{\overline{u}}_i\tilde{\overline{u}}_j)$, $\mathscr{E}_{ij}=2\{\overline{\Delta}^2|\widetilde{\overline{S}|\overline{S}}_{ij}-\tilde{\overline{\Delta}}^2|\tilde{\overline{S}}|\tilde{\overline{S}}_{ij}\}$ and the tildes denote the application of a test filter. The Taylor expansion of the $\mathscr{L}_{ij}$ term contains a term similar to the $-\overline{\Delta}^2(\overline{S}_{ik}\overline{\Omega}_{kj}+\overline{S}_{jk}\overline{\Omega}_{ki})/12$ term, and this term is not eliminated when contraction with the $\mathscr{E}_{ij}$ term was taken. A good performance of the DSM, for representing the backward scatter in particular (Piomelli *et al.* 1991), may be partly attributed to the retention of this term.

4. Characteristic features of the identified term

In the previous section, the term which is primarily responsible for causing a non-alignment of the eigenvectors for the SGS stress tensor and the strain-rate tensor was identified as the term, $-\overline{\Delta}^2(\overline{S}_{ik}\overline{\Omega}_{kj}+\overline{S}_{jk}\overline{\Omega}_{ki})/12$. In this section, we conduct a detailed investigation on the characteristics of the identified term to reveal the role of this term in turbulence generation.

The correlation between the exact τ_{ij} term and the term modelled using the nonlinear model was very high ($\rho\approx 0.91$). The correlation between the exact τ_{ij} term and the $\overline{\Delta}^2(\overline{S}_{ik}\overline{S}_{kj}-\overline{\Omega}_{ik}\overline{\Omega}_{kj})/12$ term was low (≈ 0.51), whereas that between the exact τ_{ij} term and the $-\overline{\Delta}^2(\overline{S}_{ik}\overline{\Omega}_{kj}+\overline{S}_{jk}\overline{\Omega}_{ki})/12$ terms was high (≈ 0.75), indicating that the $-\overline{\Delta}^2(\overline{S}_{ik}\overline{\Omega}_{kj}+\overline{S}_{jk}\overline{\Omega}_{ki})/12$ term is primarily responsible for the high correlation incurred by the nonlinear model.

Analytical solutions of the eigenvalues for the matrix which consists of the $-(\overline{S}_{ik}\overline{\Omega}_{kj}+\overline{S}_{jk}\overline{\Omega}_{ki})$ term in the flow with unidirectional vorticity ($\overline{\omega}_+=\overline{\omega}_-=0$), can be obtained using the matrix $\boldsymbol{L}$ as

$$\left.\begin{aligned}[-(\overline{S}_{ik}\overline{\Omega}_{kj}+\overline{S}_{jk}\overline{\Omega}_{ki})]_z&=0,\\ [-(\overline{S}_{ik}\overline{\Omega}_{kj}+\overline{S}_{jk}\overline{\Omega}_{ki})]_+&=-[-(\overline{S}_{ik}\overline{\Omega}_{kj}+\overline{S}_{jk}\overline{\Omega}_{ki})]_-.\end{aligned}\right\}\tag{4.1}$$

When the eigenvalues of the $-\overline{\Delta}^2(\overline{S}_{ik}\overline{\Omega}_{kj}+\overline{S}_{jk}\overline{\Omega}_{ki})/12$ term were obtained using the filtered DNS data described in § 2, the eigenvalue in the stretching (z-)direction was mostly close to zero (figure not shown). This result is consistent with the analytical

solutions shown in (4.1), implying that the $-(\overline{S}_{ik}\overline{\Omega}_{kj} + \overline{S}_{jk}\overline{\Omega}_{ki})$ term makes only a minor contribution to the development of the stress in the stretching (z-)direction, but contributes significantly to the development in the azimuthal directions ($+$, $-$).

Although the $-\overline{\Delta}^2(\overline{S}_{ik}\overline{\Omega}_{kj} + \overline{S}_{jk}\overline{\Omega}_{ki})/12$ term vanishes in the total production term, P, the contribution of this term is not eliminated when the generation of the vorticity is considered using the generation term for the SGS enstrophy, $(\overline{\omega_i\omega_i} - \overline{\omega}_i\overline{\omega}_i)/2 (= \overline{\Omega_{ij}\Omega_{ij}} - \overline{\Omega}_{ij}\overline{\Omega}_{ij})$, owing to the τ_{ij} term,

$$P_\omega = \varepsilon_{ilm}\overline{\omega}_i \frac{\partial^2 \tau_{mj}}{\partial x_l \partial x_j}. \tag{4.2}$$

This result indicates that the evolution of turbulent energy and enstrophy due to the $-\overline{\Delta}^2(\overline{S}_{ik}\overline{\Omega}_{kj} + \overline{S}_{jk}\overline{\Omega}_{ki})/12$ term does not take place simultaneously, but occurs with a slight time-lag. Kerr *et al.* (1996) showed that the interaction of the grid-scale velocity and the SGS vorticity is correlated strongly with the SGS transfer term, (3.3). An existence of time-lag (or phase-lag) was shown for the Kolmogorov flow (Borue & Orszag 1996), in which the signals for the turbulent energy and enstrophy were strongly coherent with a characteristic phase shift. In Yakhot (2003), it was shown that self-sustained nonlinear oscillation of energy and enstrophy describes the process of energy and enstrophy production. Although the results shown in Borue & Orszag (1996) and Yakhot (2003) were obtained in turbulence with mean shear, intense local grid-scale shear which arises even in LES of a turbulent flow without mean shear may cause similar effects on the local evolution of the SGS energy and enstrophy. An explanation for the occurrence of this time-lag was provided in Borue & Orszag (1996): the total energy dissipation rate is strongly correlated with the time derivative of the total energy, while the total dissipation rate is proportional to the total enstrophy. An alternative explanation is that the velocity field is generated by the vortex via the Biot-Savart law (Yakhot 2003). Although the generation of time-lag may be more significant in turbulence with mean shear than in that without mean shear, these two explanations are applicable to the turbulence without mean shear as well. We consider that the occurrence of this time-lag may be primarily attributed to the $-\overline{\Delta}^2(\overline{S}_{ik}\overline{\Omega}_{kj} + \overline{S}_{jk}\overline{\Omega}_{ki})/12$ term.

For both the turbulent energy and enstrophy, although a mean direction of their transfer is from the grid scale components to the SGS components (forward scatter), the SGS component is transferred in the opposite direction to the grid scale (backward scatter) as well. It was found that the backward scatter of the SGS enstrophy is correlated with the backward scatter of the SGS energy. Figure 12 shows distributions of p.d.f.s for the SGS enstrophy generation term due to the $-\overline{\Delta}^2(\overline{S}_{ik}\overline{\Omega}_{kj} + \overline{S}_{jk}\overline{\Omega}_{ki})/12$ term ((4.2) with $\tau_{ij} = -\overline{\Delta}^2(\overline{S}_{ik}\overline{\Omega}_{kj} + \overline{S}_{jk}\overline{\Omega}_{ki})/12$) taken by conditionally sampling for forward scatter events ($P > 0$) and for backward scatter events ($P < 0$). It can be seen that the p.d.f.s are skewed to positive values when $P > 0$, whereas they are skewed to negative values when $P < 0$. This result implies that the backward generation of grid-scale vorticity due to the $-\overline{\Delta}^2(\overline{S}_{ik}\overline{\Omega}_{kj} + \overline{S}_{jk}\overline{\Omega}_{ki})/12$ term is associated with the backward scatter of the SGS energy. On the whole, the p.d.f. for the P_ω term due to the $-\overline{\Delta}^2(\overline{S}_{ik}\overline{\Omega}_{kj} + \overline{S}_{jk}\overline{\Omega}_{ki})/12$ term was skewed to the negative value. When the $-\overline{\Delta}^2(\overline{S}_{ik}\overline{\Omega}_{kj} + \overline{S}_{jk}\overline{\Omega}_{ki})/12$ term was removed from the τ_{ij} term, the p.d.f. was skewed to predominantly positive values (figure not shown).

In Langford & Moser (1999), it was shown that the grid-scale statistics obtained using the various SGS models are equivalent as long as the SGS energy transfer takes place correctly, indicating that accurate representation of vorticity generation is not

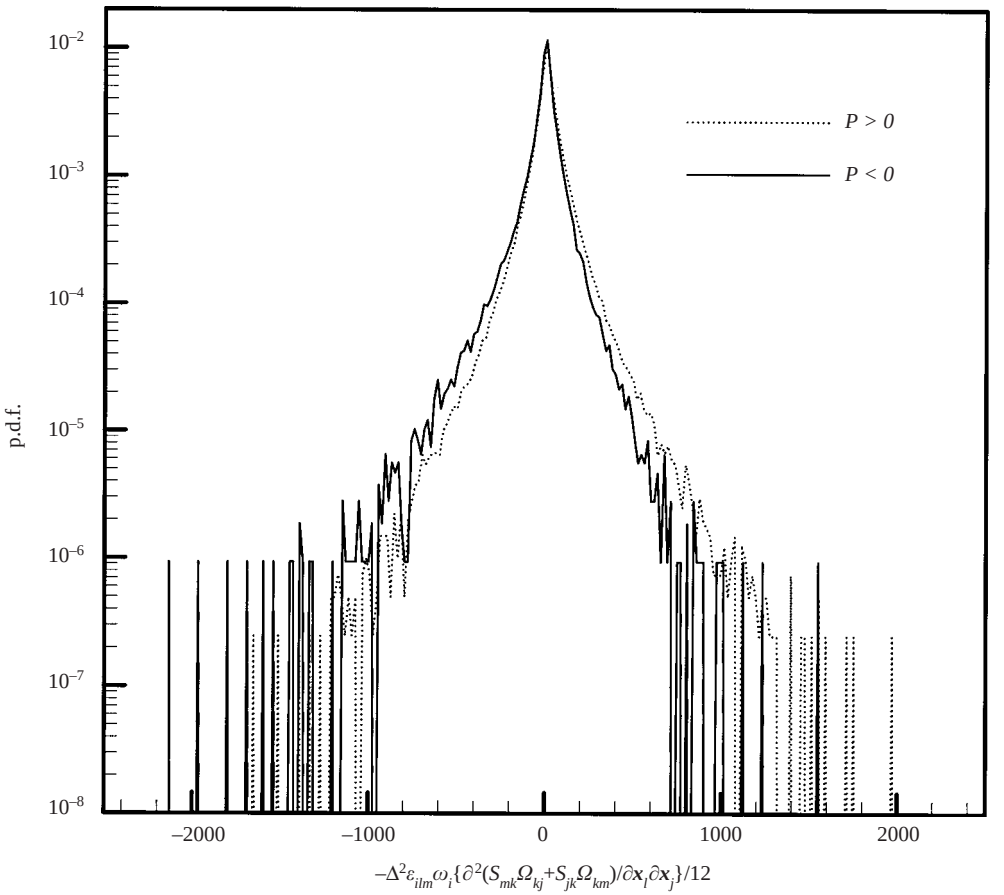

FIGURE 12. Distributions of p.d.f. for the SGS enstrophy generation term (equation (13)) due to the $-\overline{\Delta}^2(\overline{S}_{ik}\overline{\Omega}_{kj}+\overline{S}_{jk}\overline{\Omega}_{ki})/12$ term, which was conditionally sampled on the sign of P.

indispensable to achieve an optimal SGS model. Elimination of the $-\overline{\Delta}^2(\overline{S}_{ik}\overline{\Omega}_{kj}+\overline{S}_{jk}\overline{\Omega}_{ki})/12$ term in the P term and its retention in the P_ω term may be insignificant. In Langford & Moser (1999), however, the SGS energy transfer term, (3.1), was used to analyse the energy production, whereas the P term was used in the present study. It should be noted that the SGS transfer term contains the contribution of the $-\overline{\Delta}^2(\overline{S}_{ik}\overline{\Omega}_{kj}+\overline{S}_{jk}\overline{\Omega}_{ki})/12$ term since the $-\overline{\Delta}^2(\overline{S}_{ik}\overline{\Omega}_{kj}+\overline{S}_{jk}\overline{\Omega}_{ki})/12$ term does not vanish in the transfer term. Moreover, in Langford & Moser (1999), the optimal SGS model was derived using not the SGS transfer term itself, (3.1), but its correlation as $\langle\overline{u}_i(\boldsymbol{\xi})(\partial\tau_{ij}/\partial x_j)(\boldsymbol{\xi}+\boldsymbol{x})\rangle$, where $\boldsymbol{\xi}=(\xi_i)$, and $\langle f\rangle$ denotes the volume average of f in the entire domain. The optimal model obtained in Langford & Moser (1999) was the same as a spectral eddy-viscosity model.

It was shown using figure 11 that when the $-\overline{\Delta}^2(\overline{S}_{ik}\overline{\Omega}_{kj}+\overline{S}_{jk}\overline{\Omega}_{ki})/12$ term was removed from the τ_{ij} term, the eigenvectors for the SGS stress and strain-rate tensors are aligned. When the p.d.f. for the alignment between the eigenvector for the $-(\tau_{ij}+\overline{\Delta}^2(\overline{S}_{ik}\overline{\Omega}_{kj}+\overline{S}_{jk}\overline{\Omega}_{ki})/12)$ term, $-[\boldsymbol{\tau}+\overline{\Delta}^2(\boldsymbol{S\Omega}+\boldsymbol{S\Omega})/12]_i$, and the strain-rate eigenvector, $\boldsymbol{e}_i$ was taken by conditionally sampling on $P>0$, the distribution of the p.d.f. was similar to that shown in figure 11, but the two eigenvectors were more strongly aligned (figure not shown). When the p.d.f. was taken by conditionally

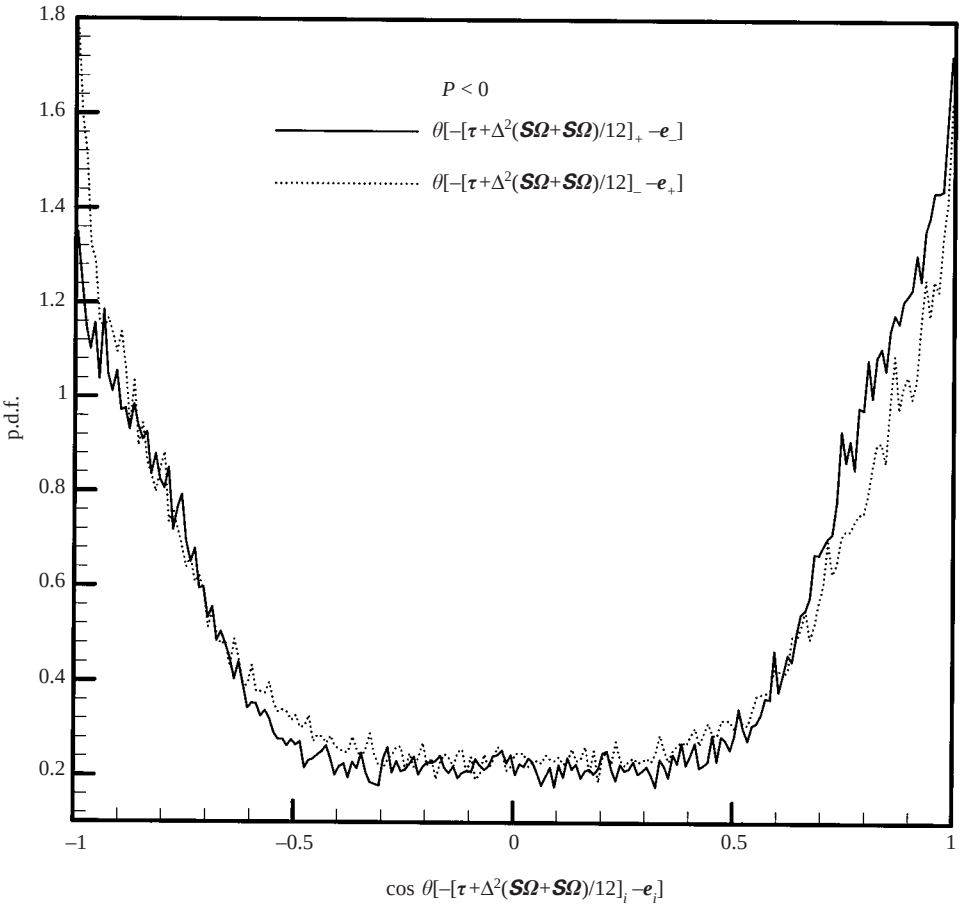

FIGURE 13. Distribution of p.d.f. for the alignment between the eigenvector for the $-(\tau_{ij} + \overline{\Delta}^2(\overline{S}_{ik}\overline{\Omega}_{kj} + \overline{S}_{jk}\overline{\Omega}_{ki})/12)$ term and the strain-rate eigenvector, $\boldsymbol{e}_i$ obtained by conditionally sampling on $P < 0$.

sampling on $P < 0$, the interchange of alignment of these two eigenvectors took place as shown in figure 13, which shows the p.d.f.s for $\cos\theta[-[\boldsymbol{\tau} + \overline{\Delta}^2(\boldsymbol{S\Omega} + \boldsymbol{S\Omega})/12]_+ - \boldsymbol{e}_-]$ and $\cos\theta[-[\boldsymbol{\tau} + \overline{\Delta}^2(\boldsymbol{S\Omega} + \boldsymbol{S\Omega})/12]_- - \boldsymbol{e}_+]$. Therefore, the eigenvectors $-[\boldsymbol{\tau} + \overline{\Delta}^2(\boldsymbol{S\Omega} + \boldsymbol{S\Omega})/12]_\pm$ and $\boldsymbol{e}_\pm$, respectively, are highly aligned when conditionally sampled on $P > 0$, but when $P < 0$, the eigenvectors, $-[\boldsymbol{\tau} + \overline{\Delta}^2(\boldsymbol{S\Omega} + \boldsymbol{S\Omega})/12]_\pm$, are not aligned with $\boldsymbol{e}_\pm$, respectively, but are aligned with $\boldsymbol{e}_\mp$, respectively, indicating that the use of a negative eddy-viscosity coefficient to represent the backward scatter is not feasible, and it should be represented by the interchange of alignment of the eigenvectors. Thus, the SGS eddy-viscosity model possesses another limitation in that the backward scatter cannot be represented using this model.

In Tao *et al.* (2002), it was shown that the angle which the eigenvector for the SGS stress tensor, $(-\boldsymbol{\tau})_1$, makes with $\boldsymbol{e}_1$, $\theta[(-\boldsymbol{\tau})_1 - \boldsymbol{e}_1]$, of peak probability was increased to $\approx 55°$, when this angle was conditionally sampled on the intense backward scatter events ($P \leqslant -\langle P \rangle$). Consistency of this value (55°) with a theoretical estimate of the angle using the approximate equation for the production term was presented. The strain state which was assumed in Tao *et al.* (2002) was that $\sigma_3 = -2\sigma_1$. This assumption may not be appropriate, since the derivative skewness,

$-\sigma_1\sigma_2\sigma_3 = -(\overline{S}_{ik}\overline{S}_{kj}\overline{S}_{ji})/3$ (equation (3.6)), which indicates the degree of strength of the energy cascade into the small scale becomes positive ($= 2\sigma_1^3 > 0$), while the $-\sigma_1\sigma_2\sigma_3$ term is generally negative when the backward scatter occurs.

We provide here an alternative explanation for the increase of the angle in the backward scatter events. In figure 6(*b*), we showed the sketch of the alignment configuration for the eigenvectors which was determined by conditionally sampling on the backward scatter events ($P < 0$). When $P < 0$, the angle which the eigenvector for the $(-\tau_{ij})$ term, $(-\boldsymbol{\tau})_+$, forms with $\boldsymbol{e}_+$, $\theta[(-\boldsymbol{\tau})_+ - \boldsymbol{e}_+]$, is intermediate between the angle $\theta[[\overline{\Delta}^2(\boldsymbol{S\Omega} + \boldsymbol{S\Omega})/12]_+ - \boldsymbol{e}_+](\approx 45^\circ)$ and the angle $\theta[-[\boldsymbol{\tau} + \overline{\Delta}^2(\boldsymbol{S\Omega} + \boldsymbol{S\Omega})/12]_+ - \boldsymbol{e}_+]$ $(\approx 90^\circ)$ because of the interchange of alignment, i.e. $45^\circ < \theta[(-\boldsymbol{\tau})_+ - \boldsymbol{e}_+] < 90^\circ$. The angle obtained in the present study was $\approx 48^\circ$, although this angle was dependent on the decomposed regions of the curved sheet, the flat sheet and the tube core. We consider that the difference in the angle obtained for the sample condition, $P > 0$, and the angle obtained for $P < 0$ is primarily attributed to the interchange of alignment of the eigenvectors $-[\boldsymbol{\tau} + (\overline{\Delta}^2(\boldsymbol{S\Omega} + \boldsymbol{S\Omega})/12)]_\pm$ and $\boldsymbol{e}_\pm$. The angle obtained in Tao *et al.* (2002) $(\approx 55^\circ)$ was slightly larger than the present value, but in both Tao *et al.* (2002) and the present study, the summation of the angles for the cases $P > 0$ and $P < 0$ was $\approx 90^\circ$.

It can be readily seen in the $-\overline{\Delta}^2(\overline{S}_{ik}\overline{\Omega}_{kj} + \overline{S}_{jk}\overline{\Omega}_{ki})/12$ term that this term takes a large value in the region where the amplitudes of strain-rate and vorticity are comparable and large, such as the Burgers vortex-layer. To examine this property of the $-\overline{\Delta}^2(\overline{S}_{ik}\overline{\Omega}_{kj} + \overline{S}_{jk}\overline{\Omega}_{ki})/12$ term, we derived the analytical eigenvalue solutions for Burgers vortex models. The eigenvalue of the $-(\overline{S}_{ik}\overline{\Omega}_{kj} + \overline{S}_{jk}\overline{\Omega}_{ki})$ term, $[-(\overline{S}_{ik}\overline{\Omega}_{kj} + \overline{S}_{jk}\overline{\Omega}_{ki})]_+$, can be obtained for the Burgers vortex-layer as

$$[-(\overline{S}_{ik}\overline{\Omega}_{kj} + \overline{S}_{jk}\overline{\Omega}_{ki})]_+ = \alpha^2 Re_\delta \exp\left(-\frac{\alpha y^2}{2\nu}\right)\sqrt{Re_\delta^2 \exp\left(-\frac{\alpha y^2}{\nu}\right) + 1}, \tag{4.3}$$

where α denotes the stretching parameter, $Re_\delta (= \sqrt{\pi/2}U_0/\sqrt{\alpha\nu})$ is the Reynolds number based on the strength of strain, U_0, and y is the distance from the centre of the layer (Horiuti 2001). Figure 14(*a*) shows the y-distributions of the eigenvalue, $[-(\overline{S}_{ik}\overline{\Omega}_{kj} + \overline{S}_{jk}\overline{\Omega}_{ki})]_+$, and the eigenvalues for the λ_2 method, $\lambda_\pm$, obtained for the Burgers vortex-layer model where α was chosen to be equal to 1.0, $\nu = 0.25$, and $Re_\delta = 10$. As was expected, the eigenvalue, $[-(\overline{S}_{ik}\overline{\Omega}_{kj} + \overline{S}_{jk}\overline{\Omega}_{ki})]_+$, is markedly large near the centre of the layer where $\lambda_+ \geqslant 0 \geqslant \lambda_-$, and decreases vary rapidly away from the centre.

For the Burgers vortex tube, the eigenvalue, $[-(\overline{S}_{ik}\overline{\Omega}_{kj} + \overline{S}_{jk}\overline{\Omega}_{ki})]_+$, can be given as

$$[-(\overline{S}_{ik}\overline{\Omega}_{kj} + \overline{S}_{jk}\overline{\Omega}_{ki})]_+ = \alpha^2 Re_\Gamma^2\ g(r)\left(\frac{4\nu}{\alpha r^2}\{1 - g(r)\} - g(r)\right),\ g(r) = \exp\left(-\frac{\alpha r^2}{4\nu}\right), \tag{4.4}$$

where $Re_\Gamma (= \Gamma/(4\pi\nu))$ is the Reynolds number based on the circulation around the tube, Γ, and r is the distance from the centre of the tube. Figure 14(*b*) shows the r-distributions of the eigenvalue, $[-(\overline{S}_{ik}\overline{\Omega}_{kj} + \overline{S}_{jk}\overline{\Omega}_{ki})]_+$, and the λ_2 eigenvalues, $\lambda_\pm$, obtained for the Burgers vortex-tube model in which α was set equal to 0.02, $\nu = 0.25$ and $Re_\Gamma = 50$. It can be seen that the eigenvalue, $[-(\overline{S}_{ik}\overline{\Omega}_{kj} + \overline{S}_{jk}\overline{\Omega}_{ki})]_+$, is very small near the centre of the tube, where $0 > \lambda_+ \geqslant \lambda_-$ (tube core), and in the curved-sheet region of the tube where $\lambda_+ \geqslant \lambda_- > 0$.

These results show that the eigenvalue, $[-(\overline{S}_{ik}\overline{\Omega}_{kj} + \overline{S}_{jk}\overline{\Omega}_{ki})]_+$, is very large in the vicinity of the centre of the vortex sheet similar to the Burgers vortex layer, i.e. the flat

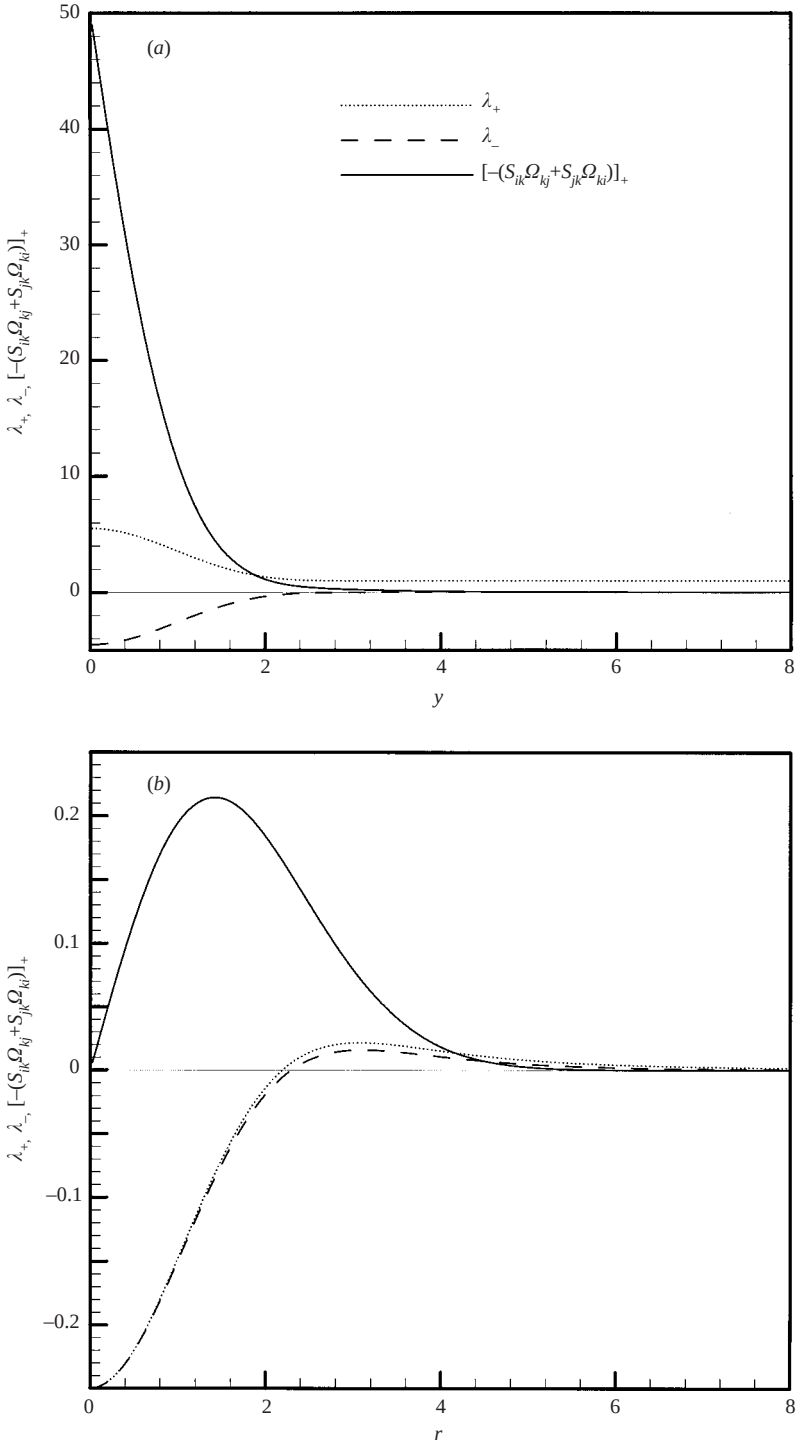

FIGURE 14. y-distributions of the reordered λ_2 eigenvalues, $\lambda_\pm$, and the eigenvalue of the $-(\overline{S}_{ik}\overline{\Omega}_{kj} + \overline{S}_{jk}\overline{\Omega}_{ki})$ term, $-[\overline{S}_{ik}\overline{\Omega}_{kj} + \overline{S}_{jk}\overline{\Omega}_{ki}]_+$: ($a$) obtained for the Burgers vortex-layer model ($\alpha = 1.0$, $\nu = 0.25$, $Re_\delta = 10$), and (b) obtained for the Burgers vortex-tube model ($\alpha = 0.02$, $\nu = 0.25$, $Re_\Gamma = 50$).

sheet. We note that although the magnitude of the eigenvalue, $[-(\overline{S}_{ik}\overline{\Omega}_{kj}+\overline{S}_{jk}\overline{\Omega}_{ki})]_+$, is very small at the centre of the vortex tube, it becomes large near the outer edge of the core region of the tube ($r \approx 1.2$ in figure 14*b*).

The eigenvalue, $[-(\overline{S}_{ik}\overline{\Omega}_{kj}+\overline{S}_{jk}\overline{\Omega}_{ki})]_+$ can be used to identify the flat sheet. Although the flat sheet can be identified using the isosurfaces of the λ_- eigenvalue with negative values (Horiuti 2001), when this eigenvalue was used, the tube core as well as the flat sheet were identified. For identifying the flat sheet by isolating it from the tube core, the isosurfaces for the eigenvalue, $[-(\overline{S}_{ik}\overline{\Omega}_{kj}+\overline{S}_{jk}\overline{\Omega}_{ki})]_+$, perform better than those of λ_-.

In figure 7, it can be seen that the probability for $\cos\theta[(-\boldsymbol{\tau})_- - \boldsymbol{e}_-] \approx 1$ in the curved-sheet region is much larger than those in the flat-sheet and tube-core regions, indicating that the occurrence of alignment between $(-\boldsymbol{\tau})_-$ and $\boldsymbol{e}_-$ is more frequent in the curved-sheet region. The alignment of $(-\boldsymbol{\tau})_-$ and $\boldsymbol{e}_-$ can be discernible in figure 4(*b*), and also a weak peak at $\cos\theta[(-\boldsymbol{\tau})_1 - \boldsymbol{e}_1] \approx 1$ and $\zeta[(-\boldsymbol{\tau})_2 - \boldsymbol{e}_2^P] \approx 0$ in figure 1 indicates that this alignment occasionally takes place. Because of the reduction of the magnitude of the $-\overline{\Delta}^2(\overline{S}_{ik}\overline{\Omega}_{kj}+\overline{S}_{jk}\overline{\Omega}_{ki})/12$ term which causes non-alignment of $(-\boldsymbol{\tau})_-$ and $\boldsymbol{e}_-$ in the curved-sheet region, $(-\boldsymbol{\tau})_-$ and $\boldsymbol{e}_-$ are more aligned in the curved-sheet region than in the flat-sheet and tube-core regions. Since the magnitude of the $-\overline{\Delta}^2(\overline{S}_{ik}\overline{\Omega}_{kj}+\overline{S}_{jk}\overline{\Omega}_{ki})/12$ term becomes rather large near the outer edge of the tube-core region, the effect of the $-\overline{\Delta}^2(\overline{S}_{ik}\overline{\Omega}_{kj}+\overline{S}_{jk}\overline{\Omega}_{ki})/12$ term is large in the tube-core region, which induces a non-alignment as in the flat-sheet region.

We mentioned in § 2 that the most probable alignment angle between the strain-rate and SGS stress eigenvectors depends on the truncation of the number of grid points from the DNS data into that of the LES data. We consider that the alignment angle depends on the degree of resolution of the flat-sheet region yielded by the LES mesh, i.e. the more finely the flat-sheet region is resolved on the LES mesh, the closer the angle is to 45°. The difference in the preferred alignment angle obtained in the present study and those in Tao *et al.* (2000) and Tao *et al.* (2002) may be partly attributed to this dependence on the resolution.

5. *A posteriori* assessment of roles of identified term

In this section, we carry out an *a posteriori* assessment of the result obtained in § 4 to elucidate the role of the identified term, $-\overline{\Delta}^2(\overline{S}_{ik}\overline{\Omega}_{kj}+\overline{S}_{jk}\overline{\Omega}_{ki})/12$, in the actual development of a turbulence field.

This *a posteriori* assessment was carried out in LES of ABC flow. DNS data for the ABC flow were generated using 135, 135 and 135 grid points, respectively, in the x-, y- and z-directions, in which the initial values were the same as those used in the previous study (Horiuti 2001). ν was set equal to 1/250. The initial values used for LES computations were those obtained by filtering the initial data of DNS using the Gaussian filter, where 135, 135 and 135 grid points were used, respectively, in the x-, y- and z-directions.

Three cases of LES calculations were considered using the variants of the nonlinear model. In Case I, the nonlinear model, (3.1), was used. Although it was shown in the previous section that the $-\overline{\Delta}^2(\overline{S}_{ik}\overline{\Omega}_{kj}+\overline{S}_{jk}\overline{\Omega}_{ki})/12$ term does not alter the production term for the total SGS energy, it may not necessarily mean that the removal of the $-\overline{\Delta}^2(\overline{S}_{ik}\overline{\Omega}_{kj}+\overline{S}_{jk}\overline{\Omega}_{ki})/12$ term does not have any influence on the temporal evolution of the turbulence field, since the $-\overline{\Delta}^2(\overline{S}_{ik}\overline{\Omega}_{kj}+\overline{S}_{jk}\overline{\Omega}_{ki})/12$ term alters the generation of the SGS vorticity. Taking into account the results shown in §4, it can be suggested

that the process of energy cascade may be enhanced or attenuated by modifying the process for generation of the SGS vorticity due to the $-\overline{\Delta}^2(\overline{S}_{ik}\overline{\Omega}_{kj}+\overline{S}_{jk}\overline{\Omega}_{ki})/12$ term. This modification can be carried out independently on the P term since the $-\overline{\Delta}^2(\overline{S}_{ik}\overline{\Omega}_{kj}+\overline{S}_{jk}\overline{\Omega}_{ki})/12$ term vanishes in the P term.

Thus, we considered the variants of the nonlinear model in which the weighting coefficients for the $-\overline{\Delta}^2(\overline{S}_{ik}\overline{\Omega}_{kj}+\overline{S}_{jk}\overline{\Omega}_{ki})/12$ term were modified. In Case II, the $-\overline{\Delta}^2(\overline{S}_{ik}\overline{\Omega}_{kj}+\overline{S}_{jk}\overline{\Omega}_{ki})/12$ term was removed from the nonlinear model, and in Case III, the $-\overline{\Delta}^2(\overline{S}_{ik}\overline{\Omega}_{kj}+\overline{S}_{jk}\overline{\Omega}_{ki})/12$ term was retained, but its sign was reversed as

$$\tau_{ij} \simeq \tfrac{1}{12}\overline{\Delta}^2\{(\overline{S}_{ik}\overline{S}_{kj}-\overline{\Omega}_{ik}\overline{\Omega}_{kj})+(\overline{S}_{ik}\overline{\Omega}_{kj}+\overline{S}_{jk}\overline{\Omega}_{ki})\}. \tag{5.1}$$

The same numbers of grid points were used for LES calculations because it was found that when the number of grid points was smaller than 135, the numerical result became unstable. To avoid this instability, the eddy-viscosity model had to be added, but it was anticipated that the alignment of eigenvectors may be obscured by adding the eddy-viscosity model because of its complete alignment with the strain-rate tensors.

In figure 15(a), the temporal variations of the grid-scale energy, $K_G(=\langle\overline{u}_i\overline{u}_i\rangle/2)$, are shown. For comparison, the results obtained from the filtered DNS data are included. The values of K_G as well as other statistical values obtained from Case II were intermediate between those from Cases I and III. Therefore, in figure 15(a) and the figures displayed in the following, the results obtained from Case II are not shown.

Figure 15(b) shows the temporal variations of the grid-scale enstrophy, $\langle\overline{\omega}_i\overline{\omega}_i\rangle$. The magnitude of enstrophy, and subsequently the dissipation rate, obtained from Case III is smaller than that from Case I when $t<5.2$. The difference in the magnitudes of the enstrophy obtained from Cases I and III is large, indicating that the $-\overline{\Delta}^2(\overline{S}_{ik}\overline{\Omega}_{kj}+\overline{S}_{jk}\overline{\Omega}_{ki})/12$ term has a noticeable influence on the generation of the vorticity.

The grid-scale vortex-stretching term, $\overline{\Omega}_{ik}\overline{\Omega}_{kj}\overline{S}_{ji}$, can be decomposed as

$$\overline{\Omega}_{ik}\overline{\Omega}_{kj}\overline{S}_{ji} = \tfrac{1}{4}\left(\sigma_z\overline{\omega}_z^2+\sigma_+\overline{\omega}_+^2+\sigma_-\overline{\omega}_-^2\right), \tag{5.2}$$

where the $\sigma_z\overline{\omega}_z^2/4$ term is the component in the stretching (z-)direction, and $\sigma_+\overline{\omega}_+^2/4$ and $\sigma_-\overline{\omega}_-^2/4$ are the components in the azimuthal directions.

It was found that the profiles of the grid-scale vortex-stretching terms as well as the SGS enstrophy generation terms, (4.2), were significantly different when different SGS models were used. Figures 16(a) and 16(b), respectively, show the p.d.f. for the z-component of the grid-scale vortex-stretching term, $\sigma_z\overline{\omega}_z^2$, and that for the grid-scale vortex-stretching term in the azimuthal direction, $\sigma_+\overline{\omega}_+^2$, which were obtained from Cases I and III at $t=3.2$. This result indicates that although the SGS production terms, P, which were yielded using the different models in Cases I, II and III are the same for the velocity fields given at one instance, the temporal developments of the velocity and vorticity fields are not the same in these three models. It can be seen in figures 16(a) and 16(b) that the amplitudes of the grid-scale vortex-stretching terms obtained from Case III are markedly smaller than those obtained from Case I.

To elucidate the implication of this difference in the magnitudes of the vortex-stretching terms, we analysed the difference in the properties of turbulent vortical structures generated in Cases I and III. It was shown in Horiuti (2001) and Horiuti *et al.* (2003) that the vortex tubes are frequently generated along the vortex sheet as follows. At certain locations along the flat sheet, compression of the vorticity in the stretching (z-) direction takes place. The occurrence of this compression is discernible in figure 16(a), in which the distribution of the p.d.f. for the $\sigma_z\overline{\omega}_z^2$ term shows large

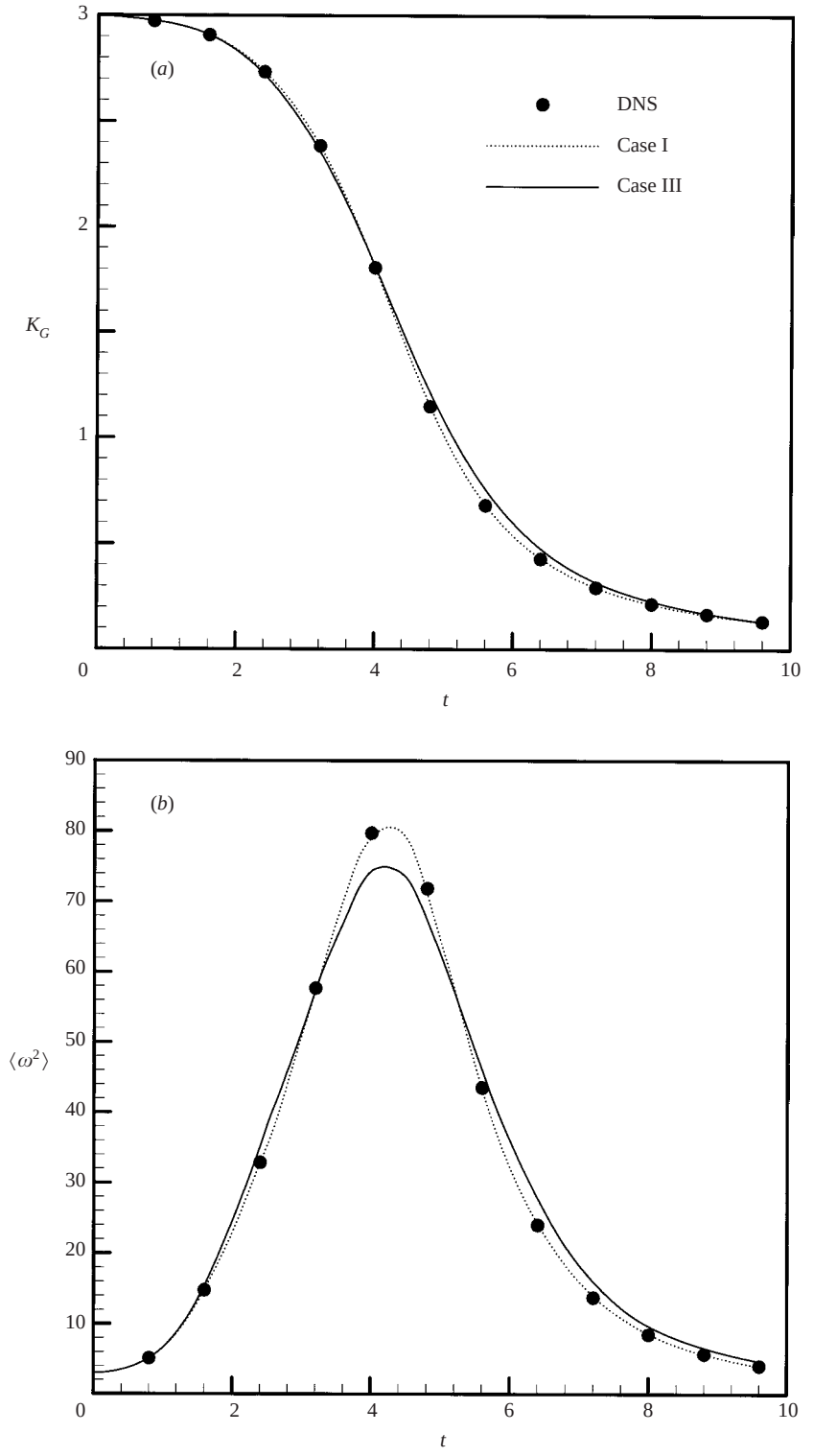

FIGURE 15. Temporal variations of turbulence statistics, which were obtained from Cases I and III and the filtered DNS data: (*a*) the grid-scale energy, K_G, and (*b*) the grid-scale enstrophy.

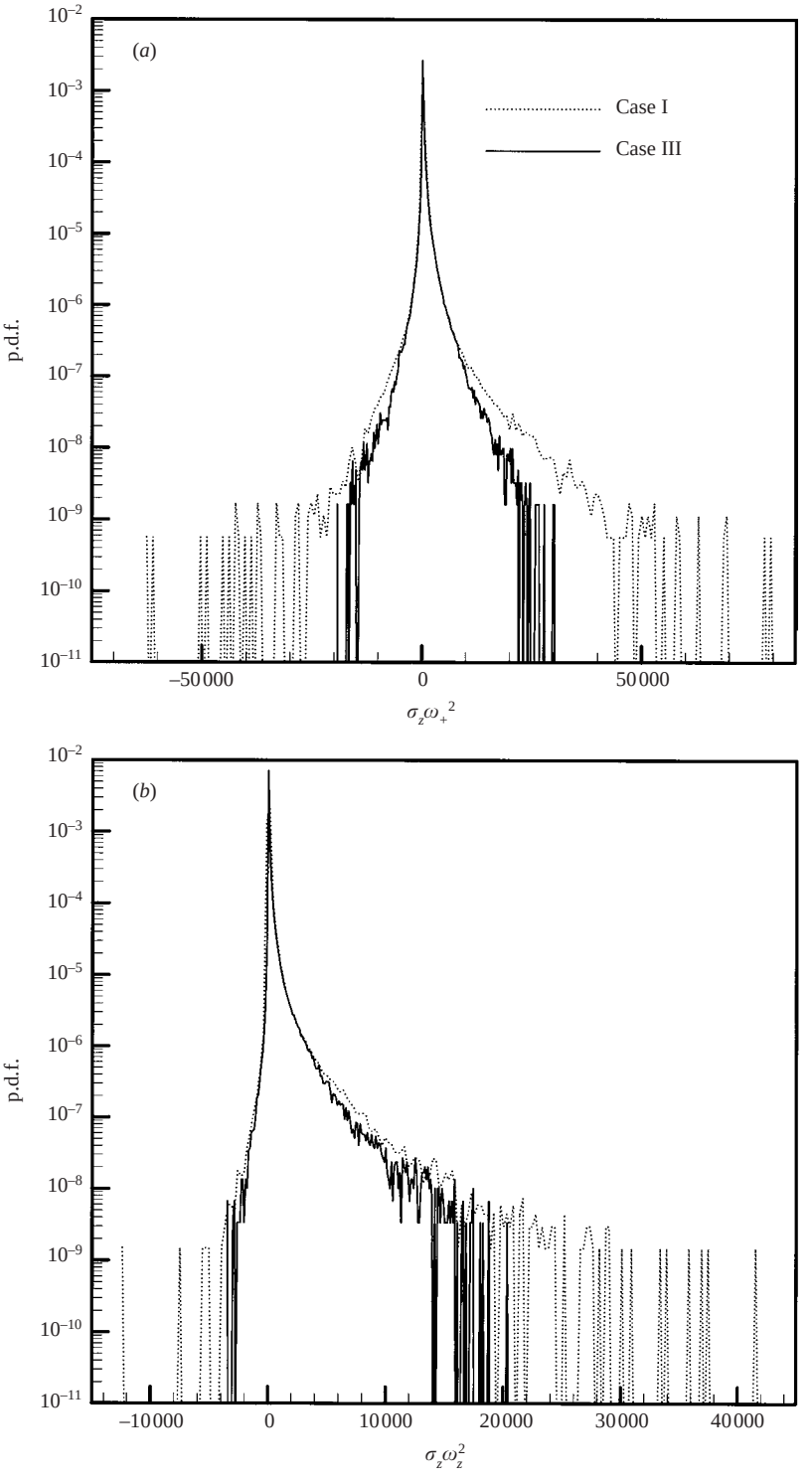

FIGURE 16. Distributions of p.d.f.s for the grid-scale vortex stretching term, which were obtained from Cases I and III at $t = 3.2$: (*a*) the z-component, $\sigma_z\overline{\omega}_z^2$, and (*b*) the azimuthal component, $\sigma_+\overline{\omega}_+^2$.

negative values (Horiuti 2000). In place of the compression and reduction of the vorticity in the z-direction, the azimuthal vorticity in the + direction grows since the $\sigma_+\overline{\omega}_+^2$ term is predominantly positive, as can be seen in figure 16(b). This growth is concentrated along the sheet, and the azimuthal vorticity gradually accumulates to form the vortex tube through a focusing process. Then, the flat sheet folds around this concentrated vortex tube, forming the spiral vortex sheet emanating from the tube core. Thus, for this process of transformation of the flat sheet into the vortex tube, the grid-scale vortex-stretching terms, in particular, the negative $\sigma_z\overline{\omega}_z^2$ term and positive $\sigma_+\overline{\omega}_+^2$ term, play critical roles. We note that this process is different from the focusing of vorticity considered by Neu (1984), in which the assumed direction of vorticity for the tube was always the z-direction.

The reason for the appearance of the alignment configuration in the flat-sheet region shown in figure 9 is not known. Its analysis will be left for future work, but we note that the joint p.d.f. shown in figure 8 exhibits broader peaks with lower magnitudes. We consider that this broad p.d.f. was generated because the flat sheet is unstable against small disturbances, and tends to be transformed into the vortex tube.

Because the amplitudes of vorticity and strain were comparable and large along the flat sheet, during this process of focusing, the generation of intense vorticity and strain and a subsequent energy cascade took place along the flat sheet (Vincent & Meneguzzi 1994; Horiuti 2001). Because a significant reduction of the amplitude of the grid-scale vortex-stretching terms takes place in Case III, the occurrence of transformation of the flat sheet into the vortex tube and subsequent turbulence generation were markedly more suppressed in Case III than in Case I.

Figure 17(a) shows the distribution of the p.d.f.s for the second-order invariant of the grid-scale velocity gradient, $Q(= -(\overline{S}_{ik}\overline{S}_{ki} + \overline{\Omega}_{ik}\overline{\Omega}_{ki})/2)$. It can be seen that the amplitude of Q obtained from Case III is smaller than that from Case I. A marked reduction of positive Q in Case III indicates that formation of the vorticity-dominant region, i.e. the vortex tube, occurs more rarely in Case III than in Case I, and the circulation around the tube obtained in Case III is weaker than that obtained in Case I. This result can be seen clearly in figure 18, which displays the isosurfaces for Q obtained from Cases I (figure 18a) and III (figure 18b) at $t = 4.8$. Tube structures which were generated in Case III are distributed more sparsely than in Case I, and the length of the vortex tubes observed in Case III is generally shorter than that observed in Case I.

As discussed in the previous section, the flat sheet can be identified using the eigenvalue of the $-\overline{\Delta}^2(\overline{S}_{ik}\overline{\Omega}_{kj} + \overline{S}_{jk}\overline{\Omega}_{ki})/12$ term, $[-\overline{\Delta}^2(\overline{S}_{ik}\overline{\Omega}_{kj} + \overline{S}_{jk}\overline{\Omega}_{ki})/12]_+$. Figure 17($b$) shows the distribution of the p.d.f. for the eigenvalue, $[-\overline{\Delta}^2(\overline{S}_{ik}\overline{\Omega}_{kj} + \overline{S}_{jk}\overline{\Omega}_{ki})/12]_+$, obtained from Cases I and III. The value of $[-\overline{\Delta}^2(\overline{S}_{ik}\overline{\Omega}_{kj}+\overline{S}_{jk}\overline{\Omega}_{ki})/12]_+$ is larger in Case III than in Case I, which indicates that the flat sheets are actually generated in Case III, and the generation is more abundant than in Case I. Figures 19(a) and 19(b), respectively, show the isosurfaces for the eigenvalue, $[-\overline{\Delta}^2(\overline{S}_{ik}\overline{\Omega}_{kj} + \overline{S}_{jk}\overline{\Omega}_{ki})/12]_+$, obtained from Cases I and III at $t = 4.8$. These figures show that formation of the sheet-like structure in Case III occurs more frequently than in Case I, but its transformation into the tube is suppressed.

It was found in Case I that the production term, P, and the SGS enstrophy generation term, P_ω, due to the $-\overline{\Delta}^2(\overline{S}_{ik}\overline{\Omega}_{kj} + \overline{S}_{jk}\overline{\Omega}_{ki})/12$ term (equation (4.2) with $\tau_{ij} = -\overline{\Delta}^2(\overline{S}_{ik}\overline{\Omega}_{kj} + \overline{S}_{jk}\overline{\Omega}_{ki})/12$), were positively correlated ($\rho \approx 0.68$), and the value of the P_ω term was skewed to positive value when $P > 0$, and to negative value when $P < 0$ (figure not shown), implying that the SGS enstrophy is generated in association

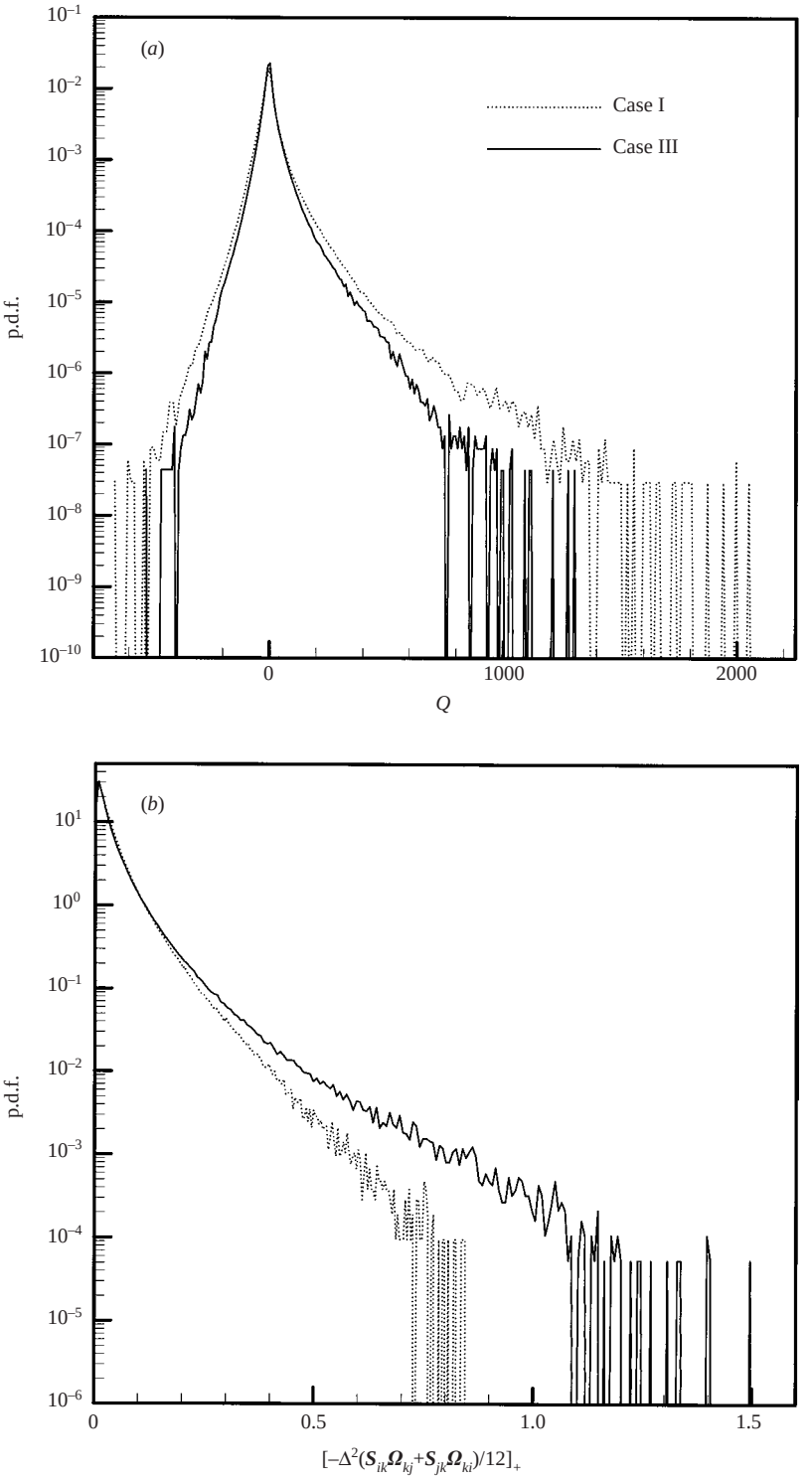

FIGURE 17. Distributions of p.d.f.s which were obtained from Cases I and III at $t = 3.2$: (*a*) for the second-order invariant of the velocity gradient tensor, Q, and (*b*) for the eigenvalue of the $-\overline{\Delta}^2(\overline{S}_{ik}\overline{\Omega}_{kj} + \overline{S}_{jk}\overline{\Omega}_{ki})/12$ term, $[-\overline{\Delta}^2(\overline{S}_{ik}\overline{\Omega}_{kj} + \overline{S}_{jk}\overline{\Omega}_{ki})/12]_+$.

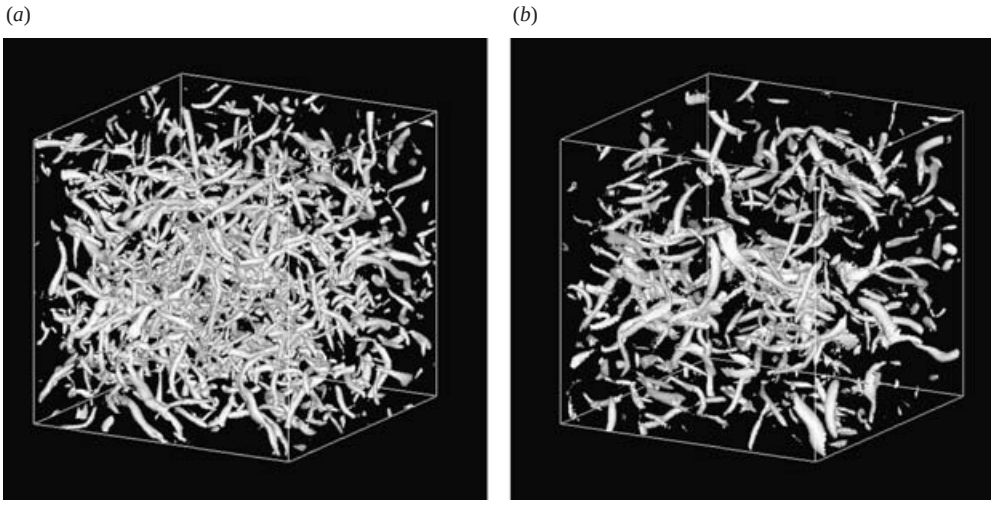

FIGURE 18. Isosurfaces of Q at $t = 4.8$: (*a*) Case I, and (*b*) Case III (isosurface level is 120 for both figures). The entire computational domain is shown.

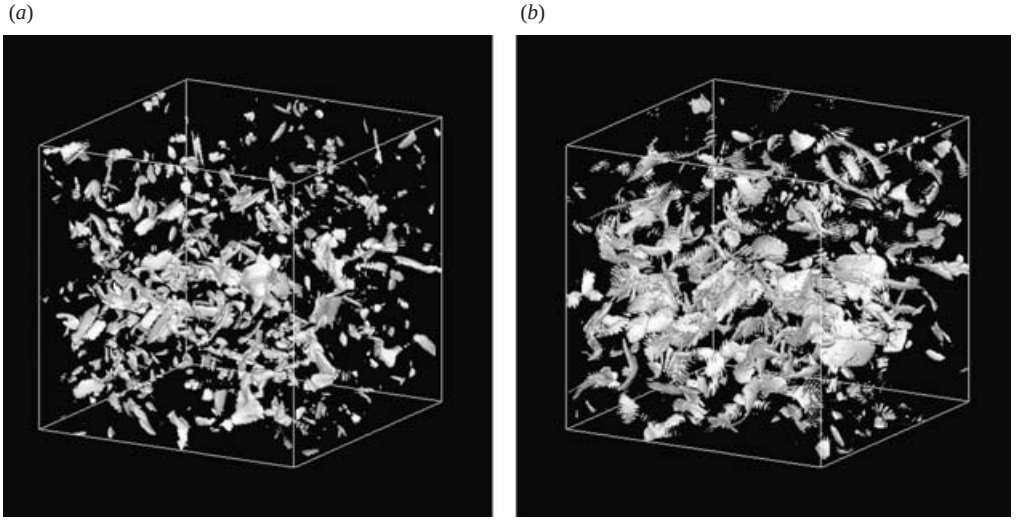

FIGURE 19. Isosurfaces of the eigenvalue of the $-\overline{\Delta}^2(\overline{S}_{ik}\overline{\Omega}_{kj} + \overline{S}_{jk}\overline{\Omega}_{ki})/12$ term, $[-\overline{\Delta}^2(\overline{S}_{ik}\overline{\Omega}_{kj} + \overline{S}_{jk}\overline{\Omega}_{ki})/12]_+$, at $t = 4.8$: (*a*) Case I, and (*b*) Case III (isosurface level is 0.2 for both figures). The entire computational domain is shown.

with the forward scatter of the grid-scale energy, and the grid-scale enstrophy is generated reversely from the SGS with the backward scatter of the SGS energy into the grid scale. This result is consistent with that obtained in the *a priori* assessment shown in § 4. Contrary to Case I, P and P_ω were negatively correlated ($\rho \approx -0.25$) in Case III (figure not shown). Therefore, in Case III, the direction of the energy cascade was inconsistent with the direction of the SGS enstrophy cascade, i.e. the SGS enstrophy was inversely cascaded to the grid scale even when the grid-scale energy was forwardly cascaded into the SGS. Therefore, the process for energy generation was disrupted by the $-\overline{\Delta}^2(\overline{S}_{ik}\overline{\Omega}_{kj} + \overline{S}_{jk}\overline{\Omega}_{ki})/12$ term in Case III, which occurred

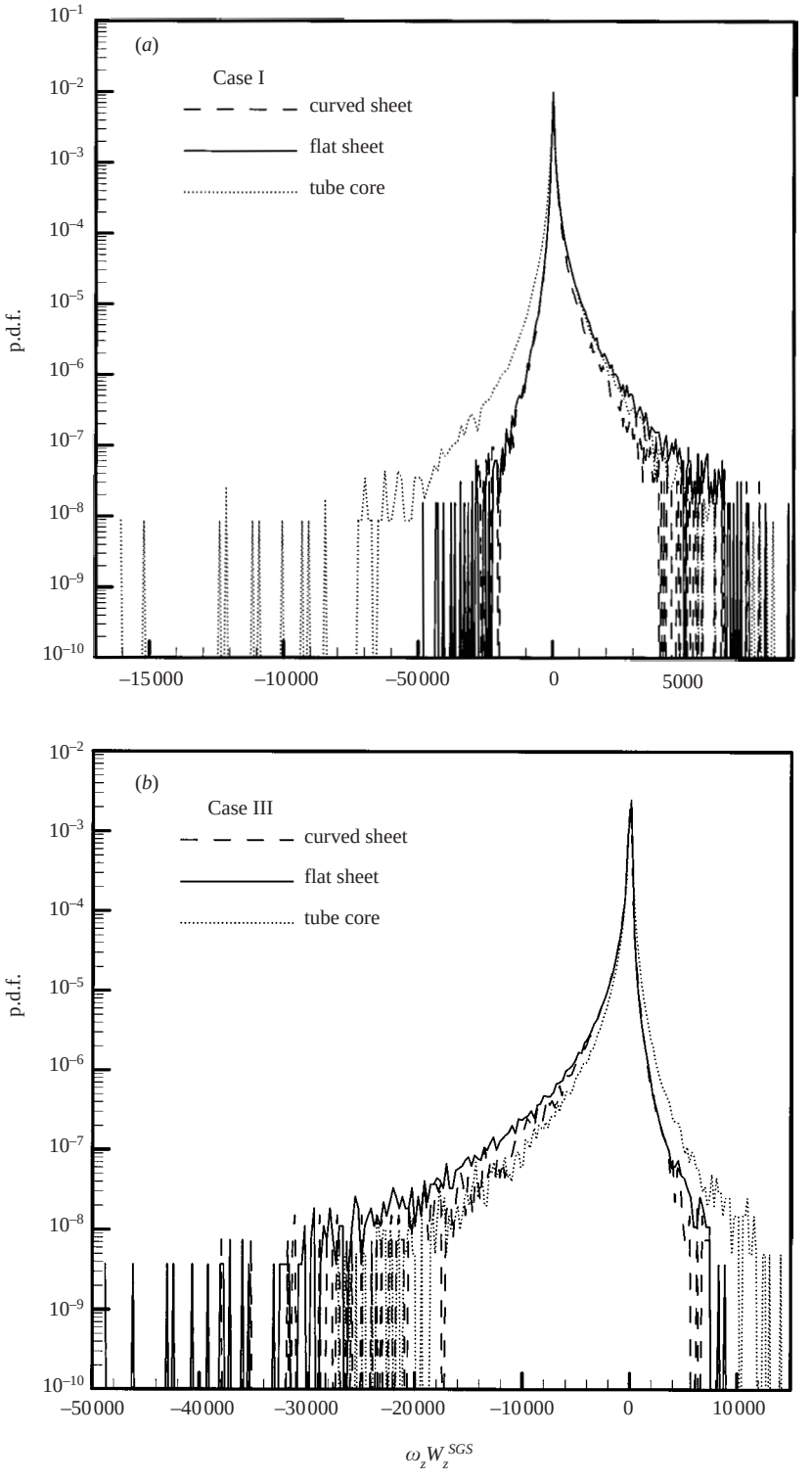

FIGURE 20. Distributions of p.d.f.s for the z-component of the SGS enstrophy generation term, $\overline{\omega}_z W_z^{\mathrm{SGS}}$, due to the $-\overline{\Delta}^2(\overline{S}_{ik}\overline{\Omega}_{kj} + \overline{S}_{jk}\overline{\Omega}_{ki})/12$ term: (*a*) Case I, and (*b*) Case III.

owing to the suppression of the occurrence of the sheet-tube transformation process in Case III.

The SGS enstrophy generation term, P_ω (equation (4.2)), can be written as the inner product of the vorticity vector, $\boldsymbol{\omega}$, with the SGS vortex-stretching vector, $\boldsymbol{W}_i^{\mathrm{SGS}}$, the ith component of which is $W_i^{\mathrm{SGS}}(=\varepsilon_{ilm}(\partial^2\tau_{mj}/\partial x_l/\partial x_j))$. When $\boldsymbol{\omega}$ and $\boldsymbol{W}_i^{\mathrm{SGS}}$ are projected onto the basis of the strain-rate eigenvectors, $\boldsymbol{e}_+$, $\boldsymbol{e}_-$, $\boldsymbol{e}_z$, P_ω can be decomposed as

$$P_\omega = \overline{\omega}_z W_z^{\mathrm{SGS}} + \overline{\omega}_+ W_+^{\mathrm{SGS}} + \overline{\omega}_- W_-^{\mathrm{SGS}}. \tag{5.3}$$

Figure 20 shows the p.d.f.s for the z-component of this decomposed P_ω term, $\overline{\omega}_z W_z^{\mathrm{SGS}}$, due to the $-\overline{\Delta}^2(\overline{S}_{ik}\overline{\Omega}_{kj}+\overline{S}_{jk}\overline{\Omega}_{ki})/12$ term, in which τ_{ij} was set equal to $-\overline{\Delta}^2(\overline{S}_{ik}\overline{\Omega}_{kj}+\overline{S}_{jk}\overline{\Omega}_{ki})/12$. Figures 20(a) and 20(b) are from Cases I and III, respectively. The p.d.f.s were decomposed into those in the curved-sheet, flat-sheet and tube-core regions. In Case I, the SGS enstrophy was backwardly transferred into the grid scale selectively in the tube core region, while it was forwardly transferred into the SGS on average in the other two regions, indicating that the role of the $-\overline{\Delta}^2(\overline{S}_{ik}\overline{\Omega}_{kj}+\overline{S}_{jk}\overline{\Omega}_{ki})/12$ term is to enhance the generation of the core region of the vortex tube. In Case III, the SGS enstrophy was backwardly transferred into the grid scale in all three regions, but the most intense backward transfer occurred in the flat-sheet region, indicating that the grid-scale vorticity in the stretching (z-)direction is strengthened in the flat-sheet region. As a result, in Case III, the $-\overline{\Delta}^2(\overline{S}_{ik}\overline{\Omega}_{kj}+\overline{S}_{jk}\overline{\Omega}_{ki})/12$ term tends to disrupt the transformation of the flat sheet into the vortex tube by snapping the sheet back to the original flat shape. We note that the distributions for p.d.f.s for the z-component of the P_ω term due to the $\overline{\Delta}^2(\overline{S}_{ik}\overline{S}_{kj}-\overline{\Omega}_{ik}\overline{\Omega}_{kj})/12$ term were skewed to positive values in both Cases I and III (figure not shown).

The results obtained from Case I shown above were close to those obtained from the filtered DNS data, indicating that the original nonlinear model works best, and an improper treatment of the $-\overline{\Delta}^2(\overline{S}_{ik}\overline{\Omega}_{kj}+\overline{S}_{jk}\overline{\Omega}_{ki})/12$ term yields incorrect results for LES of the Newtonian fluids. We note, however, that disruption of the energy cascade and the subsequent reduction of formation of tube structures observed in Case III is similar to the phenomenon of the drag reduction by dilute polymer additives (e.g. Sureshkumar, Beris & Handel 1997). The relationship between the variant of the nonlinear model which was used in Case III and the Oldroyd constitutive equation which provides a fair representation of a viscoelastic fluid (Oldroyd 1950) is reported in Horiuti *et al.* (2003).

6. Conclusions

We have studied alignment of the eigenvectors for the strain-rate tensor and the subgrid-scale (SGS) stress tensor in large-eddy simulation (LES). In the *a priori* assessment, their alignment was investigated using the direct numerical simulation (DNS) data for incompressible homogeneous isotropic turbulence. By applying the filtering operation to the DNS data, the exact SGS stress tensor and strain-rate tensor were derived.

We reordered the eigenvalues according to the degree of alignment of the corresponding eigenvectors with the vorticity vector. As stated in the previous reports of Tao, Katz & Meneveau (2000, 2002), the eigenvectors of the strain-rate and SGS stress tensors were seen to be strongly non-aligned. The most probable alignment

configuration determined in the present study was similar to that obtained in Tao *et al.* (2002), but the angle which the non-aligned eigenvectors form was $\approx 42^\circ$, which is larger than $\approx 34^\circ$ reported in Tao *et al.* (2000) and $\approx 32^\circ$ in Tao *et al.* (2002). Using the reordering of the eigenvalues, the appearance of bimodal behaviour of the alignment configuration pointed out in Tao *et al.* (2002) was eliminated.

The specific term which is primarily responsible for generation of the non-alignment of the eigenvectors was identified in the decomposition of the SGS stress tensor using the nonlinear model as the $-\overline{\Delta}^2(\overline{S}_{ik}\overline{\Omega}_{kj} + \overline{S}_{jk}\overline{\Omega}_{ki})/12$ term. The angle which the $-\overline{\Delta}^2(\overline{S}_{ik}\overline{\Omega}_{kj} + \overline{S}_{jk}\overline{\Omega}_{ki})/12$ term forms with the strain-rate eigenvectors was $\approx 45^\circ$, while when the $-\overline{\Delta}^2(\overline{S}_{ik}\overline{\Omega}_{kj} + \overline{S}_{jk}\overline{\Omega}_{ki})/12$ term was removed from the SGS stress tensor, the eigenvector for the remainder was parallel to the strain-rate eigenvector.

As in Tao *et al.* (2002), the alignment trends were affected substantially by sampling conditions based on the magnitudes of the SGS production term, strain rate and vorticity. In the present study, conditional sampling was carried out based on the relative dominance of strain and vorticity. The entire region was divided into three regions, namely, the strain-dominated region (curved sheet), vorticity-dominated region (tube core) and the region in which the magnitudes of strain and vorticity are comparable and large (flat sheet) (Horiuti 2001).

The effect of the identified term on the alignment was largest in the flat-sheet region. As a result, the most probable alignment configuration in the flat-sheet region was different from those in the curved-sheet and tube-core regions. The preferred relative orientation of the strain-rate and SGS stress eigenvectors was dependent on the degree of resolution of the flat-sheet region yielded using the LES mesh. Although its occurrence was infrequent, an additional alignment configuration in which all strain-rate and stress eigenvectors were aligned was observed in the curved-sheet region since this region was least affected by the identified term.

Interchange of the alignment between the strain-rate and stress eigenvectors took place when the SGS energy was backwardly transferred to the grid scale. The alignment configuration was different from that in which the forward scatter of the grid-scale energy into the SGS took place, and the alignment angle was increased to $\approx 48^\circ$. This interchange of the alignment cannot be represented using the SGS eddy-viscosity model.

It was shown that the identified term makes no contribution to the production term for the total SGS energy, but this term is relevant for the generation of the SGS enstrophy, which occurred during the process of the formation of the vortex tube along the flat sheet through compression of the flat sheet. The effect of the identified term on the enstrophy generation was investigated in the *a posteriori* assessment by modifying the coefficient of the $-\overline{\Delta}^2(\overline{S}_{ik}\overline{\Omega}_{kj} + \overline{S}_{jk}\overline{\Omega}_{ki})/12$ term. When the sign for the coefficient of the $-\overline{\Delta}^2(\overline{S}_{ik}\overline{\Omega}_{kj} + \overline{S}_{jk}\overline{\Omega}_{ki})/12$ term was reversed, the transformation of the flat sheet into the vortex tube was markedly disrupted, and the original nonlinear model yielded the result which is in the closest agreement with the DNS data. A proper treatment of the $-\overline{\Delta}^2(\overline{S}_{ik}\overline{\Omega}_{kj} + \overline{S}_{jk}\overline{\Omega}_{ki})/12$ term is indispensable for an accurate SGS modelling.

I am grateful to S. Abe for assistance with the LES calculations. This work was partially supported by Grants-in-Aid from the Ministry of Education, Culture, Sports, Science and Technology, Japan (nos. 12650156 and 14550141). Main computations were performed using the NEC SX-5 systems at the Cybermedia Centre, Osaka University and at the Computer Centre, Tokyo Institute of Technology.

Appendix. General form of the nonlinear model

The nonlinear model has been used for the closures of the Reynolds stresses in the Reynolds averaged turbulence modelling. As was shown in Speziale (1991), the nonlinear model (equation (3.1)) can be written in a general form as

$$\tau_{ij} \simeq \alpha_1 l^2 \overline{S}_{ik}\overline{S}_{kj} + \alpha_2 l^2 \overline{\Omega}_{ik}\overline{\Omega}_{kj} + \alpha_3 l^2 (\overline{S}_{ik}\overline{\Omega}_{kj} + \overline{S}_{jk}\overline{\Omega}_{ki}), \tag{A 1}$$

where $\alpha_1, \alpha_2, \alpha_3$ are constants, and l denotes the length scale. In Speziale (1987), the constants were optimized as

$$\tau_{ij} \simeq \alpha_1 l^2 \overline{S}_{ik}\overline{S}_{kj} - \alpha_1 l^2 (\overline{S}_{ik}\overline{\Omega}_{kj} + \overline{S}_{jk}\overline{\Omega}_{ki}), \tag{A 2}$$

in which the $\overline{\Omega}_{ik}\overline{\Omega}_{kj}$ term was removed by invoking the constraint of the indifference of the stress tensor in a frame of reference undergoing rotation. This constraint may not be applicable to LES because the cutoff of the SGS is not sufficiently small so that the motion of the SGS is unaffected by rotation (Speziale 1985). α_1 was set equal to a positive value.

In Kosović (1997), the nonlinear model as

$$\tau_{ij} \simeq -C_1 l^2 \overline{S}_{ik}\overline{S}_{kj} - C_2 l^2 (\overline{S}_{ik}\overline{\Omega}_{kj} + \overline{S}_{jk}\overline{\Omega}_{ki}), \tag{A 3}$$

was used for LES of the turbulent boundary layer, where C_1, C_2 are constants. The coefficient of the $\overline{S}_{ik}\overline{S}_{kj}$ term was set to a negative value to represent the backward scatter of the SGS energy into the grid scale. It appears, however, that when the experimentally measured values of the normal stress components (equation (4.16) in Kosović 1997) are used to determine the values for C_1 and C_2, the relationship $C_2 = -C_1$ is yielded instead of $C_2 = C_1$ which was shown in (4.18) of Kosović (1997), and the value for C_1 should be set equal to a negative value to yield a positive value for the τ_{11} term. Then, the nonlinear model which is equivalent to that in (A 2) is derived. It should be noted that both in Speziale (1987) and Kosović (1997), the coefficient for the $(\overline{S}_{ik}\overline{\Omega}_{kj} + \overline{S}_{jk}\overline{\Omega}_{ki})$ term was negative, since C_2 was set to a positive value. In all studies cited in Speziale (1991) which dealt with the nonlinear model, the coefficient for the $(\overline{S}_{ik}\overline{\Omega}_{kj} + \overline{S}_{jk}\overline{\Omega}_{ki})$ term was set to a negative value.

REFERENCES

Andreotti, B. 1997 Studying Burgers' models to investigate the physical meaning of the alignments statistically observed in turbulence. *Phys. Fluids* **9**, 735.

Ashurst, W. T., Kerstein, A. R., Kerr, R. M. & Gibson, C. H. 1987 Alignment of vorticity and scalar gradient with strain rate in simulated Navier–Stokes turbulence. *Phys. Fluids* **30**, 2343.

Bardina, J. 1983 Improved turbulence models based on large eddy simulation of homogeneous, incompressible turbulent flows. PhD thesis, Stanford University.

Batchelor, G. K. 1967 *An Introduction to Fluid Mechanics*. Cambridge University Press.

Borue, V. & Orszag, S. A. 1996 Numerical study of three-dimensional Kolmogorov flow at high Reynolds numbers. *J. Fluid Mech.* **306**, 293.

Clark, R. A., Ferziger, J. H. & Reynolds, W. C. 1979 Evaluation of subgrid-scale models using an accurately simulated turbulent flow. *J. Fluid Mech.* **91**, 1.

Domaradzki, J. A. & Saiki, E. M. 1997 A subgrid-scale model based on the estimation of unresolved scales of turbulence. *Phys. Fluids* **9**, 2148.

Horiuti, K. 2000 Assessment of subgrid-scale models in dissipative vortical structures. In *Advances in Turbulence VIII* (ed. C. Dopazo), p. 519. CIMNE.

Horiuti, K. 2001 A classification method for vortex sheet and tube structures in turbulent flows. *Phys. Fluids* **13**, 3756.

Horiuti, K., Abe, S., Itami, T. & Takagi, Y. 2003 Effects of viscoelasticity and compressibility on turbulence structure formation. In *Proc. 3rd Symp. on Turbulence and Shear Flow Phenomena* (ed. N. Kasagi *et al.*), p. 823.

Jeong, J. & Hussain, F. 1995 On the identification of a vortex. *J. Fluid Mech.* **285**, 69.

Jiménez, J. 1992 Kinematic alignment effects in turbulent flows. *Phys. Fluids* A **4**, 652.

Kerr, R. M., Domaradzki, J. A. & Barbier, G. 1996 Small-scale properties of nonlinear interactions and subgrid-scale energy transfer in isotropic turbulence. *Phys. Fluids* **8**, 197.

Kosović, B. 1997 Subgrid-scale modelling for the large-eddy simulation of high-Reynolds-number boundary layers. *J. Fluid Mech.* **336**, 151.

Langford, J. A. & Moser, R. D. 1999 Optimal LES formulations for isotropic turbulence. *J. Fluid Mech.* **398**, 321.

Liu, S., Meneveau, C. & Katz, J. 1994 On the properties of similarity subgrid-scale models as deduced from measurements in a turbulent jet. *J. Fluid Mech.* **275**, 83.

Lund, T. S. & Rogers, M. M. 1994 An improved measure of strain state probability in turbulent flows. *Phys. Fluids* **6**, 1838.

Meneveau, C. & Katz, J. 2000 Scale-invariance and turbulence models for large-eddy simulation. *Annu. Rev. Fluid Mech.* **32**, 1.

Neu, J. C. 1984 The dynamics of stretched vortices. *J. Fluid Mech.* **143**, 253.

Nomura, K. K. & Post, G. K. 1998 The structure and dynamics of vorticity and rate of strain in incompressible homogeneous turbulence. *J. Fluid Mech.* **377**, 65.

Oldroyd, J. G. 1950 On the formulation of rheological equations of state. *Proc. R. Soc. Lond.* A **200**, 523.

Piomelli, U. 1999 Large-eddy simulation: achievements and challenges. *Prog. Aerospace Sci.* **35**, 335.

Piomelli, U., Cabot, W. H., Moin, P. & Lee, S. 1991 Subgrid-scale backscatter in turbulent and transitional channel flow. *Phys. Fluids* **31**, 1884.

Smagorinsky, J. 1963 General circulation experiments with the primitive equations. I. The basic experiment. *Mon. Weather Rev.* **91**, 99.

Speziale, C. G. 1985 Subgrid-scale stress models for the large eddy simulation of rotating turbulent flows. *Geophys. Astrophys. Fluid Dyn.* **33**, 199.

Speziale, C. G. 1987 On nonlinear $K-l$ and $K-\varepsilon$ models of turbulence. *J. Fluid Mech.* **178**, 459.

Speziale, C. G. 1991 Analytical methods for the development of Reynolds-stress closures in turbulence. *Annu. Rev. Fluid Mech.* **23**, 107.

Sureshkumar, R., Beris, A. N. & Handel, R. A. 1997 Direct numerical simulation of the turbulent channel flow of a polymer solution. *Phys. Fluids* **9**, 743.

Tao, B., Katz, J. & Meneveau, C. 2000 Geometry and scale relationships in high Reynolds number turbulence determined from three-dimensional holographic velocimetry. *Phys. Fluids* **12**, 941.

Tao, B., Katz, J. & Meneveau, C. 2002 Statistical geometry of subgrid-scale stresses determined from holographic velocimetry measurements. *J. Fluid Mech.* **457**, 35.

Vincent, A. & Meneguzzi, M. 1994 The dynamics of vorticity tubes in homogeneous turbulence. *J. Fluid Mech.* **258**, 245.

Yakhot, V. 2003 A simple model for self-sustained oscillations in homogeneous shear flow. *Phys. Fluids* **15**, L17.